European Journal of Medicinal Chemistry 136 (2017) 523–542

Contents lists available at ScienceDirect

European Journal of Medicinal Chemistry

journal homepage: http://www.elsevier.com/locate/ejmech

Research paper

Novel propanamides as fatty acid amide hydrolase inhibitors

Alessandro Deplano [a, 1], Carmine Marco Morgillo [c, 1], Monica Demurtas [a], Emmelie Björklund [b], Mariateresa Cipriano [b], Mona Svensson [b], Sanaz Hashemian [b], Giovanni Smaldone [d], Emilia Pedone [e], F. Javier Luque [f], Maria G. Cabiddu [g], Ettore Novellino [c], Christopher J. Fowler [b], Bruno Catalanotti [c, *], Valentina Onnis [a]

[a] Department of Life and Environmental Sciences, Unit of Pharmaceutical, Pharmacological and Nutraceutical Sciences, University of Cagliari, via Ospedale 72, Cagliari I-09124, Italy
[b] Department of Pharmacology and Clinical Neuroscience, Umeå University, SE-901 87 Umeå, Sweden
[c] Department of Pharmacy, Università Degli Studi di Napoli Federico II, Napoli, Italy
[d] IRCCS SDN, Via Emanuele Gianturco 113, 80143 Napoli, Italy
[e] Institute of Biostructures and Bioimaging, CNR, Naples, Italy
[f] Departament de Nutrició, Ciències de l'Alimentació i Gastronomia and Institut de Biomedicina (IBUB), Facultat de Farmàcia i Ciències de l'Alimentació, Universitat de Barcelona, Santa Coloma de Gramenet, Spain
[g] Department of Chemical and Geological Sciences, University of Cagliari, Italy

ARTICLE INFO

Article history:
Received 3 March 2017
Received in revised form
2 May 2017
Accepted 11 May 2017
Available online 12 May 2017

Keywords:
FAAH inhibitors
Heteroaryl propanamides
Fatty acid amide hydrolase
Endocannabinoids
Anandamide

ABSTRACT

Fatty acid amide hydrolase (FAAH) has a key role in the control of the cannabinoid signaling, through the hydrolysis of the endocannabinoids anandamide and in some tissues 2-arachidonoylglycerol. FAAH inhibition represents a promising strategy to activate the cannabinoid system, since it does not result in the psychotropic and peripheral side effects characterizing the agonists of the cannabinoid receptors. Here we present the discovery of a novel class of profen derivatives, the *N*-(heteroaryl)-2-(4-((2-(trifluoromethyl)pyridin-4-yl)amino)phenyl)propanamides, as FAAH inhibitors. Enzymatic assays showed potencies toward FAAH ranging from nanomolar to micromolar range, and the most compounds lack activity toward the two isoforms of cyclooxygenase. Extensive structure-activity studies and the definition of the binding mode for the lead compound of the series are also presented. Kinetic assays in rat and mouse FAAH on selected compounds of the series demonstrated that slight modifications of the chemical structure could influence the binding mode and give rise to competitive (**TPA1**) or non-competitive (**TPA14**) inhibition modes.

1. Introduction

Anandamide (AEA), 2-acylethanolamines and 2-arachidonoyl glycerol are signaling lipids belonging to the class of endocannabinoids, endogenous agonists of the cannabinoid receptor type-1 (CB_1) and type-2 (CB_2). The cannabinoid system regulates many physiological functions, both in the central and peripheral nervous systems and in peripheral organs. In order to maintain the normal functionality of nerve systems, many fatty acid amides, including AEA, are degraded by fatty acid amide hydrolase (FAAH), a member of the serine hydrolase enzyme family, characterized by the unusual catalytic triad Ser^{217}-Lys^{142}-Ser^{241}.

Blockade of FAAH activity is a suitable strategy to modulate the endocannabinoid system compared to exogenous cannabinoid receptor agonists, whose therapeutic profile is heavily limited by CB_1-mediated psychotropic and peripheral side effects such as impairment in cognition, motor coordination, and psychoses. It is now well established that the endocannabinoid system is involved in the regulation of mood, and in animal models of anxiety, and that FAAH inhibitors show a potentially useful profile [1]. Additionally, FAAH inhibitors may be useful in disorders ranging from cannabinoid dependence [2] to preventing or reducing the inflammatory process associated with Aβ deposition in Alzheimer's Disease [3] and in the treatment of comorbidity between psychological disorders and cardiac disease [4]. The principal classes of covalent and non-covalent inhibitors as well as the FAAH inhibitors entered into

* Corresponding author.
E-mail address: brucatal@unina.it (B. Catalanotti).
[1] These authors equally contribute to the present paper.

http://dx.doi.org/10.1016/j.ejmech.2017.05.033
0223-5234/

clinical studies have been recently reviewed [5]. Clinical studies so far undertaken indicate that FAAH inhibitors are generally well tolerated [6,7]. A serious brain injury was reported in a phase I study with the FAAH inhibitor BIA 10-2474, but this appears to be an off-target effect of the drug, not correlated to FAAH inhibition [8]. Indeed, a computer-based proteome-docking approach suggested that BIA 10-2474 could interact with several targets in a manner likely to cause brain haemorrhaging [9].

We previously reported that some NSAIDs as ibuprofen display modest FAAH inhibitory activity. The conversion of the carboxylic group of ibuprofen into heterocyclic amide namely 2-(4-isobutylphenyl)-*N*-(3-methylpyridin-2-yl)propanamide (**Ibu-AM5**) that showed high FAAH inhibitory activity, while retaining COX inhibitory properties of the parent ibuprofen [10–12]. Encouraged by these finding, we have been prompted to investigate further new **Ibu-AM5** analogs as potential FAAH inhibitors. Since superimposition of **Ibu-AM5** with FAAH co-crystallized inhibitors indicated that the isobutyl chain of **Ibu-AM5** overlap aromatic hydrophilic moieties, as a rational development we designed and synthesized a new series of compounds where the isobutyl group is replaced by a 2-(trifluoromethyl)pyridin-4-ylamino group (Fig. 1). In the present study we report the discovery, synthesis, pharmacological and biochemical characterization of these compounds, as well as their putative binding mode of the lead and finally the efforts to identify key structural features of this novel series of *N*-(heteroaryl)-2-(4-((2-(trifluoromethyl)pyridin-4-yl)amino)phenyl) propanamides as FAAH inhibitors. With the aim to define the critical requirements for FAAH inhibitory activity we have explored the effects of structural modification in the heteroaryl group, in the linker between the heteroaryl group and the phenylcarbonyl moiety, the effect of replacement of the methyl on the C-2 with smaller and larger substituents, and finally the effect of introducing different polar rings in the (trifluoromethyl)pyridine region.

2. Results and discussion

2.1. Chemistry

The synthesis of the target amides was undertaken as outlined in Schemes 1-6. The first step of the synthetic approach to the new series of TPA amides was based on a previously described procedure that allows the construction of the trifluoromethylpyridine ring linked by an amino nitrogen to an aromatic ring [13]. This synthetic approach was modified and successfully applied for the preparation of 2-(4-((2-(trifluoromethyl)pyridin-4-yl)amino)phenyl)propanoic acid (**7**) starting from the easily available 2-(4-nitrophenyl)propionic acid (**1**), which was first converted into its methyl ester and then submitted to reduction of the nitro group. The resulting methyl 2-(4-aminophenyl)propanoate **2** reacted with 1,1,1-trifluoro-4-methoxypent-3-en-2-one (**3**) in 1:1.5 molar ratio in refluxing acetonitrile (MeCN) solution to yield the enaminone **4** in good yields. Upon reacting with an excess of *N*,*N*-dimethylformamide dimethyl acetal (DMF-DMA) in refluxing toluene, the enaminone **4** was converted into 1,1,1,trifluorohexadienone **5** in 88% yield. The treatment of intermediate **5** with ammonium acetate in DMF at 100 °C produced pyridine ring closure to ester **6** in 75% yield. Hydrolysis of compound **6** in hydroalcoholic sodium hydroxide solution afforded acid **7**.

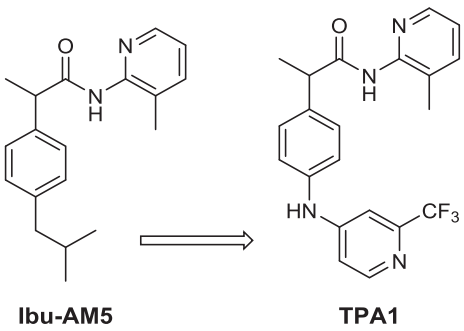

Fig. 1. Design of the representative member TPA1 from Ibu-AM5.

Finally, treatment of acid **7** with the appropriate amine in the presence of 1-(3-dimethylaminopropyl)-3-ethylcarbodiimide hydrochloride (EDC) and 1-hydroxybenzotriazole (HOBt) in MeCN solution gave amides **TPA1-16, 18-21** in moderate to good yields.

In order to study the structure-activity relationship of TPA compounds and to discover the better modification to improve the activity as FAAH inhibitors, we modified all moieties of the molecule.

First we focused our attention upon the 3-methylpyridin-2-yl moiety. To evaluate the effect of the presence of the methyl group and of its position on the pyridine ring upon the FAAH inhibitory properties. Specifically, the 2-aminopyridine, 3-aminopyridine and 4-aminopyridine analogs **TPA4-6** and the 5-methyl **TPA2** and 4-methyl **TPA3** analogs were prepared as reported in Scheme 1. To evaluate the effect of pyridine replacement by other rings, the phenyl analog **TPA7**, the pyrimidine (**TPA8**), pyrazine (**TPA9**), quinoline (**TPA10**) and arylpiperazino analogues (**TPA18–21**) were also prepared (Scheme 1). Finally, the 3-methylpyrido group was replaced with halogens and trifluoromethyl group (**TPA11–14**).

To investigate the importance for FAAH inhibition of the distance between the carbonyl group and the pyridine ring, the acid **7** was condensed with 2-picolylamine and 3-picolylamine to obtain amides **TPA15** and **TPA16** respectively (Scheme 1). Further linker extension was accomplished through introduction of a second amide moiety to give **TPA17**. As indicated in Scheme 2, **TPA17** was prepared by condensation between **7** and ethyl glycinate hydrochloride using the EDC method. The obtained ester **8** was hydrolyzed under basic conditions to obtain compound **9**. This acid was finally condensed with the 2-amino-3-methylpiridine using the EDC method to obtain the amide **TPA17.**

To examine the importance of the substituent on C-α to the carbonyl group firstly, a slight modification of the procedure used to afford acid **7** was employed. Thus, the unsubstituted derivative **TPA22** was prepared starting from the methyl ester of the 2-(4-aminophenyl)acetic acid (**10**). The obtained acid **14** was subsequently condensed with 2-amino-3-methylpyridine using EDC method (Scheme 3).

To introduce a second methyl or a cycloalkyl group on the C-α 2-(4-nitrophenyl)acetic acid was converted into its methyl ester derivative **15**, which was treated with iodomethane in DMF solution in the presence of sodium hydride to obtain intermediate **16**.The nitro group of **16** was reduced into its corresponding amine (**17**). Compound **17** was used as starting material for the construction of the trifluoromethylpyridine ring through the reaction sequence above described and then the acid **21** was converted into **TPA23** by EDC method (Scheme 4).

TPA24–27 were prepared in an analogous manner starting from the nitro derivative **15** and the appropriate di-halogen derivative, namely 1,2-dibromoethane, 1,3-diiodopropane, 1,4-diiodobutane, 1,5-diiodopentane respectively that were reacted modifying a described method [14] (Scheme 5).

Finally, we investigated the importance for FAAH inhibition of the trifluoromethylpyridine ring. To this purpose, the ester **2** was hydrolyzed to the acid **46.** That is subsequently treated with 4-chloro-8-trifluoromethylquinoline and 4-chloro-7-trifluoromethylquinoline to obtain the corresponding acids **47** and **48**, which are condensed with 2-amino-3-methylpyridine by

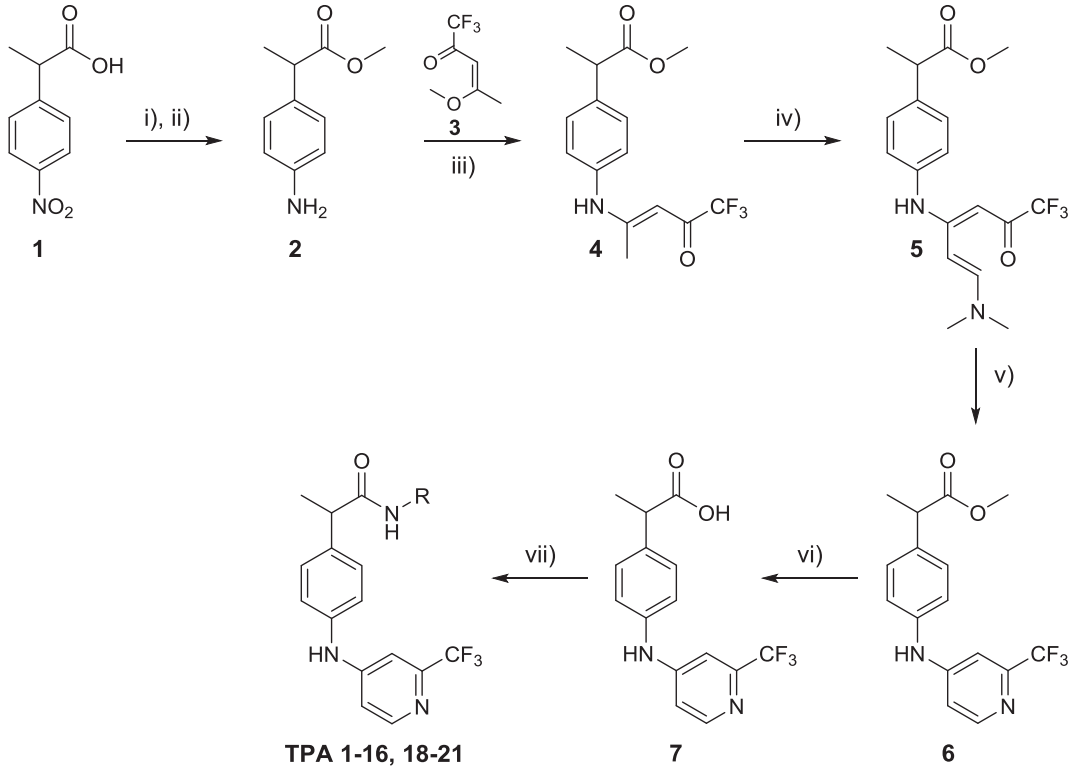

Scheme 1. Reagents and conditions: (i) MeOH, HCl 37%, reflux, 4 h; (ii) Fe, HCl 37%, MeOH, H_2O, reflux overnight; (iii) MeCN, reflux, 2 h; (iv) DMF-DMA, PhMe, reflux, 1 h; (v) NH_4OAc, DMF, reflux, 1.5 h; (vi) EtOH, 5 N aq. NaOH, r.t., 24 h; (vii) R-NH_2, EDC, HOBt, MeCN, r.t., 18–36 h.

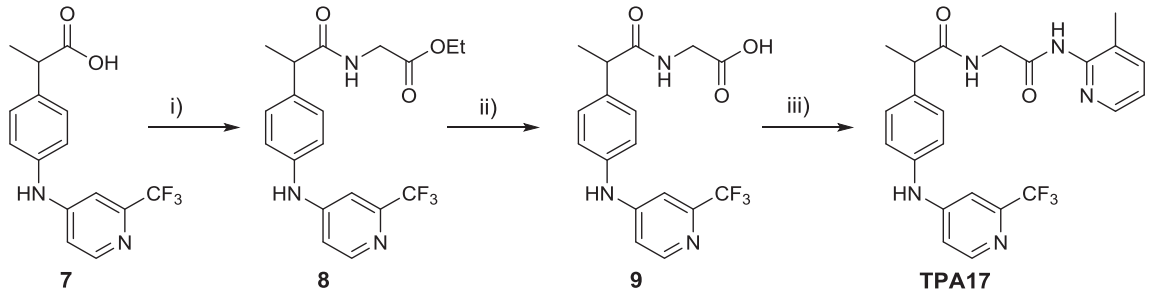

Scheme 2. Reagents and conditions: (i) Ethyl glicinate hydrochloride, EDC, HOBt, TEA, MeCN, r.t., 4 h; (ii) EtOH, 5 N aq. NaOH, r.t., 24 h; (iii) EDC, HOBt, MeCN, r.t., 36 h.

EDC method to obtain **TPA28** and **TPA29**, respectively (Scheme 6).

2.2. FAAH inhibitory activity

The racemate of compounds **TPA1-29**, along with the reference compound **Ibu-AM5**, were evaluated for their ability to inhibit FAAH. The inhibition assays were performed using 0.5 μM [^{3}H]AEA as substrate and rat brain homogenates as enzyme source. In all cases reported here, concentration-response curves were constructed from values from at least 3 experiments using at least five concentrations over the appropriate range (in half log units, i.e. 0.3, 1, 3, 10, 30, 100 μM). The results of these primary assays are showed in Tables 1, and 3-5. The replacement of the **Ibu-AM5** isobutyl chain with a trifluoromethylamino moiety to give **TPA1** led to similar inhibitory activity (IC_{50} values of 0.52 and 0.59 μM, respectively).

2.2.1. Mode of inhibition of FAAH by TPA1

To explore the inhibition mechanism, a preincubation time-course study was performed on **TPA1**. If a compound inhibits the enzyme via an irreversible mechanism, upon prolonged pre-incubation the potency should become greater; a constant IC_{50}, conversely, supports a reversible mechanism. For a fully reversible compound, the percentage of control activity seen in the green bars (i.e. following the dilution) should be higher than in the orange bars (the remaining activity seen at the undiluted concentrations) but equal to the white bars (the free concentrations after the dilution). **TPA1** showed no time-dependent increase in potency, consistent with a reversible mechanism of action (Fig. 2A). This was confirmed in dilution experiments (Fig. 2B). The kinetics of inhibition was investigated for both rat and mouse FAAH. For the rat, the data was better fitted by a model assuming a competitive mode of inhibition than by a mixed model inhibition (Fig. 2C), whereas in the mouse, the mixed model inhibition fitted the data best (Fig. 2D). The lower potency in the mouse compared to the rat has also been seen for **Ibu-AM5** and 2-(2-fluoro-(1,1'-biphenyl)-4-yl)-*N*-(3-methylpyridin-2-yl)propanamide (**Flu-AM1**) [12].

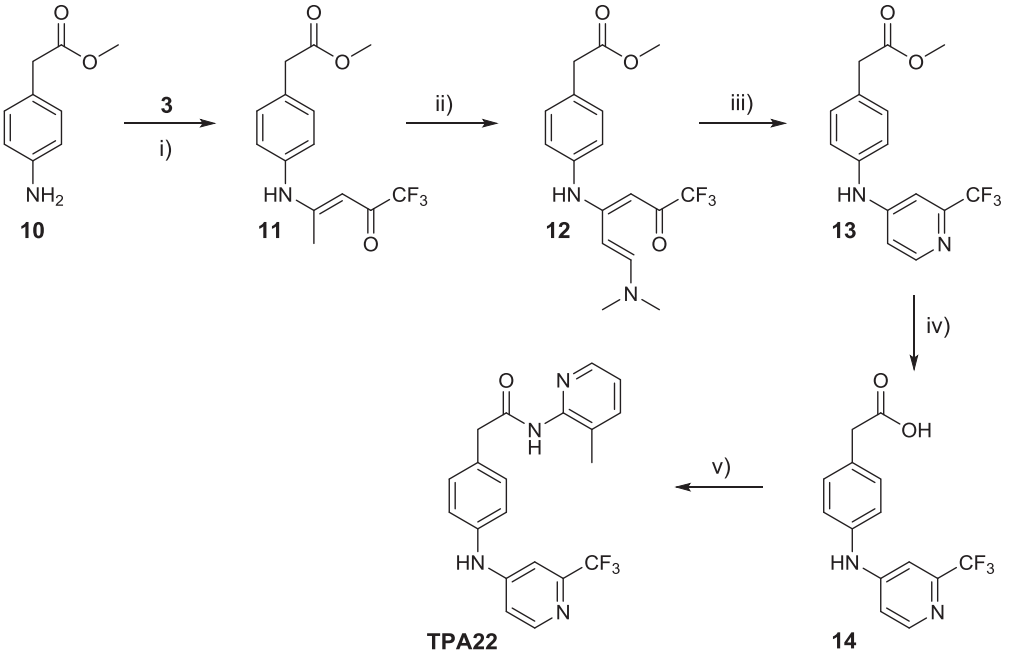

Scheme 3. Reagents and conditions: (i) MeCN, reflux, 2 h; (ii) DMF-DMA, PhMe, reflux, 1 h; (iii) NH_4OAc, DMF, reflux, 1.5 h; (iv) EtOH, 5 N aq. NaOH, r.t., 24 h; (v) EDC, HOBt, MeCN, r.t., 36 h.

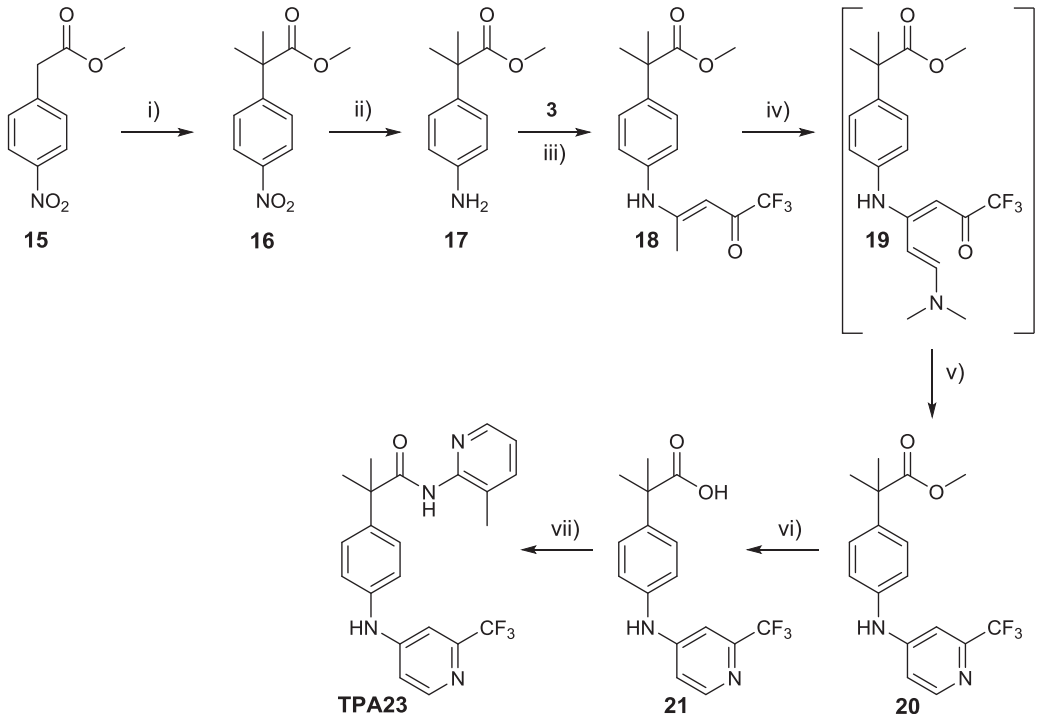

Scheme 4. Reagents and conditions: (i) MeI, NaH, DMF, 0 °C to r.t.; (ii) $SnCl_2$ $2H_2O$, EtOH, 85 °C, 4 h; (iii) MeCN, reflux, 2 h; (iv) DMF-DMA, PhMe, reflux, 1 h; (v) NH_4OAc, DMF, reflux, 1.5 h; (vi) EtOH, 5 N aq. NaOH, r.t., 24 h; (vii) EDC, HOBt, MeCN, r.t., 36 h.

2.2.2. Binding mode of TPA1

Taking into account the competitive inhibition mechanism of **TPA1** for rat FAAH, we studied its binding mode by combining docking and molecular dynamics (MD) simulations using the protocol reported previously [12]. Given that ***(S)*-Ibu-AM5** is 10-fold more potent FAAH inhibitor than ***(R)*-Ibu-AM5**, while ***(S)*-Flu-AM1** and ***(R)*-Flu-AM1** are almost equipotent, we used the *(S)*-enantiomer for computational studies on **TPA1**. Docking was performed with Autodock 4.2 targeting all the binding sites reported for known competitive inhibitors (i.e., the membrane access channel, the acyl chain binding channel, the catalytic site and the cytosolic port). The results suggest that **TPA1** preferentially binds the acyl chain binding (ABP) channel in proximity to the catalytic triad. Four arrangements that differ in the orientation and

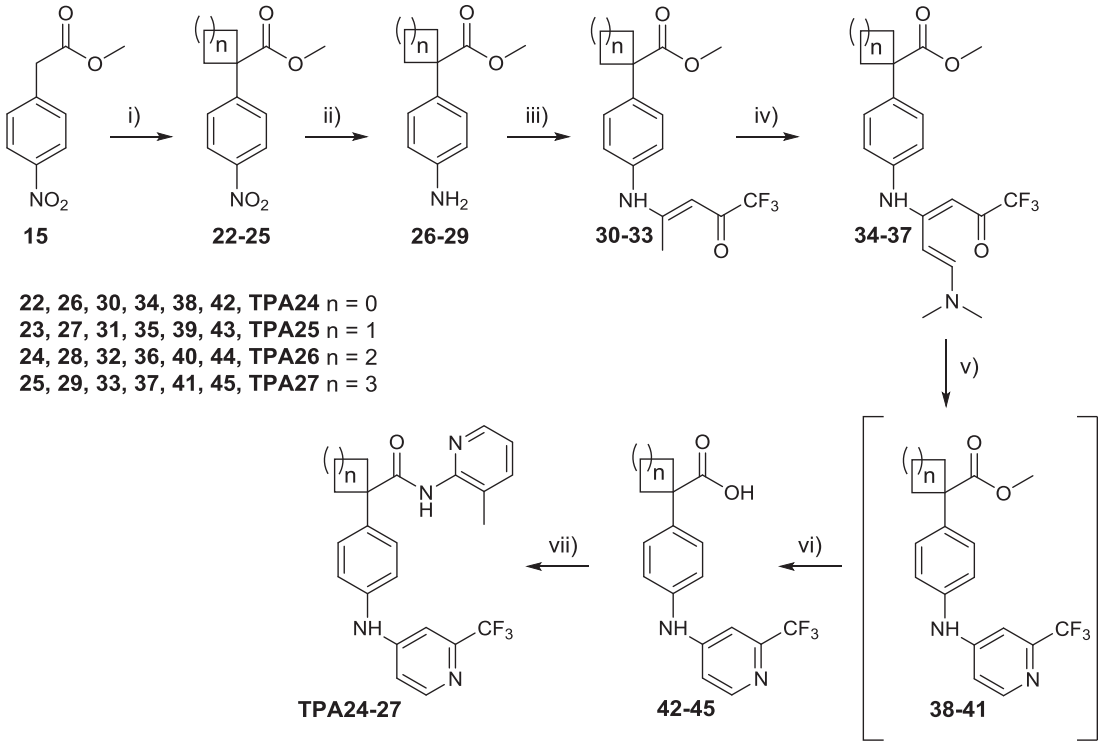

Scheme 5. Reagents and conditions: (i) DMF, NaH, di-haloalkane, 0 °C to r.t.; (ii) AcOEt, $SnCl_2$ $2H_2O$, 75 °C, 4 h; (iii) MeCN, reflux, 2 h; (iv) DMF-DMA, PhMe, reflux, 1 h; (v) NH_4OAc, DMF, reflux, 1.5 h; (vi) EtOH, 5 N aq. NaOH, r.t., 24 h; (vii) EDC, HOBt, MeCN, r.t., 36 h.

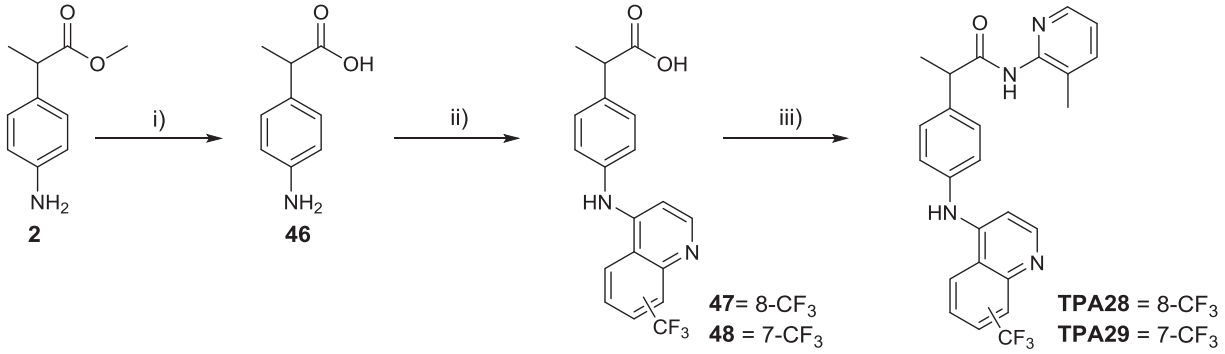

Scheme 6. Reagents and conditions: (i) EtOH, 5 N aq. NaOH, r.t., 24 h; (ii) EtOH, appropriate 4-chlorotrifluoromethylquinoline, reflux, 24 h; (iii) EDC, HOBt, MeCN, r.t., 36 h.

positioning of the ligand along the ABP channel were found (Table 2; Supplementary data Fig. S1), which have the amide moiety pointing towards the cytosolic port (A1-mode), the catalytic triad (A2-mode), the membrane access channel (B1-mode), or the membrane interacting helices α18-α19 (B2-mode). Even though binding modes A1 and B1 are the most populated clusters, encompassing 50% and 30% of the docked poses, the score of the four poses differ by less than 0.7 kcal/mol, which impedes to rule out any of the four arrangements. Therefore, we examined the structural stability of the four poses by running MD simulations (100 ns) using the dimeric form of the enzyme with the ligand loaded in the two monomers, thus allowing to enhance the statistics of our analysis.

The stability of the binding mode along the trajectory was examined by monitoring the ligand RMSD profile, and the convergence of the binding in the monomers was evaluated by comparing the main clusters. The A1-binding mode was very stable along the trajectories, (RMSD $\leq$ 1.5 Å; Supplementary data Figs. S2–A), and showed convergence toward a common binding mode in the two monomers (Figs. S1–B). On the contrary, A2, B1 and B2 binding modes underwent larger rearrangements, showing less stability and a lower degree of convergence. (RMSD $\geq$ 2.5 Å; Supplementary data Fig. S3).

To analyze further the results of the MD refinement, the binding free energies were estimated using Molecular Mechanics Generalized Born Surface Area (MM/GBSA) [15], and Solvated Interaction Energy (SIE) [16], which relies on specific parameterization of the PBSA method. The differences in binding affinity consistently supported the larger stability of the A1-binding mode. Nevertheless, taking into account that very similar compounds, such as **Flu-AM1** and **Ibu-AM5**, showed binding modes comparable to the B2-mode [12], we further assessed the interaction energy between **TPA1** and the protein using hybrid quantum mechanical molecular mechanics (QM/MM) calculations for each representative binding mode, which indicated that the A1 binding mode has the most favored interaction energy (Table 2; Supplementary data Table S1).

Table 1
FAAH Inhibitory activity of compounds TPA1-14.

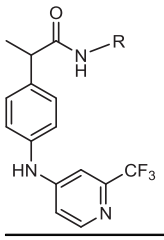

Compound	R	Max inhibition (%)	IC_{50} (μM)	pIC_{50}±s.e.m[a]
TPA1	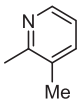	100	0.59	6.23 ± 0.03
TPA2	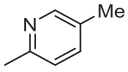	68 ± 4	11	4.95 ± 0.08
TPA3	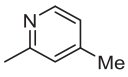	100	4.0	5.40 ± 0.01
TPA4		93 ± 3	12	4.92 ± 0.04
TPA5		86 ± 2	6.4	5.19 ± 0.04
TPA6		100	52	4.28 ± 0.08
TPA7	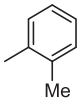	100	0.74	6.13 ± 0.02
TPA8		100	0.99	6.00 ± 0.03
TPA9		100	2.0	5.70 ± 0.04
TPA10	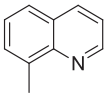	75 ± 7	4.3	5.37 ± 0.15
TPA11	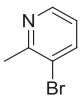	100	0.13	6.87 ± 0.03
TPA12		100	0.10	6.99 ± 0.09
TPA13	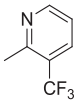	100	0.33	6.48 ± 0.02
TPA14	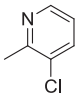	100	0.058	7.24 ± 0.02

[a] pI_{50} values (i.e.,-log10(IC_{50}) values) are indicated because the analysis method returns theseSE values, which are then antilogged to give the IC_{50} values for the inhibitable component (max inhibition) of the FAAH activity.

In the A1-mode (Fig. 3) **TPA1** binds prevalently through hydrophobic interactions with the apolar gorge of ABP, supported by few hydrogen bonds. In particular, the methyl-pyridine moiety is in the proximity of the catalytic triad, tightly packed against Met^{191}, Leu^{192}, Ile^{238}, Val^{270} and Leu^{278}. The carbonyl oxygen of the amide group is near the anionic hole formed by the main chains of residues Ile^{238}, Gly^{239}, Gly^{240} and Ser^{241}, while the NH group forms a stable hydrogen bond with the backbone of Met^{191}. The interactions of the amide group and of the methyl-pyridine ring required the adoption of a specific conformation, which is characterized by a relative torsion of 48°. This arrangement seems to be a key requisite for FAAH inhibition of this class of compounds. Further apolar interactions of the aromatic groups with lipophilic residues along the channel, including Trp^{531}, Phe^{432} and Thr^{488} and a water-bridged H-bond of aromatic and the backbone of Leu^{192} contribute to stabilize the binding.

Finally, we also compared the **TPA1** A1-binding mode with those experimentally determined for other inhibitors. **TPA1** adopts a binding conformation that matches well the structure of methyl arachidonyl fluorophosphonate (MAFP; PDB ID: 1MT5), although this latter compound binds even deeper in the MAC (Supplementary data Figs. S4–A). A similar behavior is observed from the superposition with three compounds of the series of α-ketoheterocycle covalent FAAH inhibitors [17–20]. (Supplementary data Fig. S4-B-D). In particular, the carbonyl moiety of the two compounds fills the same position, pointing towards the anionic hole, while the nitrogen on the pyridine ring of **TPA1** overlaps the nitrogen in the oxazole moiety (Supplementary data Figs. S4–D). Albeit the A1-binding mode strictly resembles that of substrates, or covalent inhibitors such as α-ketoheterocycles, the absence of time-dependency clearly showed that TPA1 is not hydrolyzed by FAAH (Fig. 2A), since such hydrolysis would have resulted in a decreasing potency with increasing preincubation time. In order to verify if conditions for a nucleophilic attack of Ser217 to the TPA1 amide group subsisted during the MD, we analyzed the geometrical features of the catalytic triad, by monitoring key generic descriptors as proposed by Palermo et al. [21]. Results demonstrated that during the whole trajectory key geometrical descriptors do not assume values suitable for a catalytic attack of the TPA1 amide bond (Supplementary data Fig. S5).

The involvement of Thr^{488} in the A1-binding mode suggests that **TPA1** binding would be affected by mutating this residue in the wild-type FAAH. This was investigated in experiments where HeLa cells transfected expressing wild-type FAAH or $FAAH^{T488A}$ were used (Supplementary data Table S2). For comparative purposes, **(*R*)-Flu-AM1** was also investigated, since previous data indicated that the potency of this compound was indeed lower towards the $FAAH^{T488A}$ mutant [12]. Even though the results might suggest a reduction in the inhibitory potency in the mutated enzyme, variation between transfection batches in the sensitivity to inhibition by **TPA1** and by **(*R*)-Flu-AM1** suggest caution in interpretation of the data (see Supplementary data).

2.2.3. SAR of TPA1 analogs

With the aim to explore the SAR of this new series of reversible FAAH inhibitors, we designed a number of derivatives to gain insight into the role of different moieties of the lead **TPA1**. In particular we explored the effect of modifications of the 3-methylpyridin-2-yl moiety, the methyl group in C-α to the carbonyl group, and the 2-(trifluoromethyl)pyridine ring.

Effect of the distance between the arylpropanoic acid core and pyridine ring. The effect of the length of the linker between the arylpropanoic acid core and pyridine ring was determined (Table 3). Insertion of a methylene unit (**TPA15** and **TPA16**) significantly reduced the inhibitory activity as compared to **TPA1**, as the

Table 2
Docking and MD refining results and analysis. In cases of non-convergent binding modes in the two monomers, data are reported for the best cluster in the monomer A (a0) and B (b0). MMGBSA, SIE and QM/MM free energy values are in kcal/mol.

DOCKING				MD analysis[b]				
mode	Pop%	AD score	MMGBSA[a]	cluster	Pop%	ΔG MMGBSA	ΔG SIE	ΔG QM/MM[c]
A1	50	−9.1	- 59.5	0	97.8	- 58.5	- 10.2	- 75.0
A2	3	−8.4	- 49.6	a0	96.2	- 48.0	- 9.3	- 57.2
				b0	38.6	- 48.6	- 9.4	- 64.7
B1	30	−9.0	- 49.2	a0	66.7	- 45.8	- 8.9	- 53.1
				b0	75.1	- 48.2	- 9.1	- 52.5
B2	9	−8.7	- 50.7	a0	94.5	- 42.4	- 8.6	- 63.3
				b0	48.7	- 47.6	- 9.3	- 59.8

[a] Estimated for the docked pose of the ligand.
[b] Values determined for a set of 50 snapshots taken on 0.1 ns along the MD trajectory.
[c] The solvation energy term (ΔGsol) was calculated by MM/GBSA.

Table 3
FAAH Inhibitory activity of compounds TPA15-21.

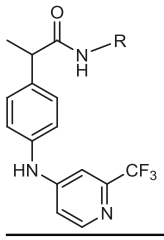

Compound	R	Max inhibition (%)	IC_{50} (μM)	pIC_{50}±s.e.m[a]
TPA15	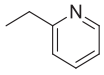	100	23	4.63 ± 0.01
TPA16	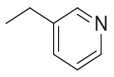	100	32	4.50 ± 0.02
TPA17	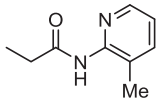	100	2.4	5.62 ± 0.01
TPA18	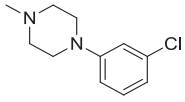	100	27	4.57 ± 0.14
TPA19	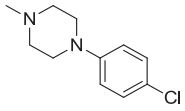	65 ± 8	17	4.76 ± 0.15
TPA20	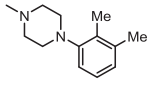	24 ± 2% inhibition at 100 μM		
TPA21	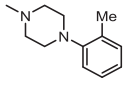	24 ± 3% inhibition at 100 μM		

[a] pI_{50} values (i.e.,-log10(IC_{50}) values) are indicated because the analysis method returns theseSE values, which are then antilogged to give the IC_{50} values for the inhibitable component (max inhibition) of the FAAH activity.

IC_{50} values increase by about 40-fold. Likewise, introduction of a piperazine ring had a similar effect (**TPA18** and **TPA19**) or even eliminated the inhibitory activity (**TPA20** and **TPA21**). In contrast, insertion of an additional amide unit (**TPA17**) still reduced the inhibitory potency, but only by a factor of 4 with respect to **TPA1**. Taken together these results indicate an ortho-substituted aromatic amide as essential for FAAH inhibitory activity.

Furthermore, the data suggest that the linker present in **TPA1** is likely to be optimal for the activity. These results are consistent with the proposed A1-binding mode, as the methyl pyridine moiety is well packed in the pocket defined by residues Met^{191}, Leu^{192}, Ile^{238}, Val^{270} and Leu^{278}, while the amide bond is involved in polar interactions with the anionic hole and the backbone of Met^{191}. Accordingly, docking of TPA15 in the FAAH showed that the

Table 4
FAAH Inhibitory activity of compounds TPA22-27.

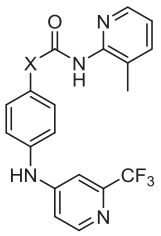

Compound	X	Max inhibition (%)	IC_{50} (μM)	pIC_{50}±s.e.m[a]
TPA22	CH_2	100	48	4.31 ± 0.06
TPA23	$C(CH_3)_2$	100	1.8	5.74 ± 0.06
TPA24		100	14	4.87 ± 0.08
TPA25		100	9.1	5.04 ± 0.05
TPA26		100	60	4.22 ± 0.13
TPA27		30 ± 3% inhibition at100 μM		

[a] pI_{50} values (i.e.,-log10(IC_{50}) values) are indicated because the analysis method returns theseSE values, which are then antilogged to give the IC_{50} values for the inhibitable component (max inhibition) of the FAAH activity.

Table 5
FAAH Inhibitory activity of compounds TPA28 and TPA29.

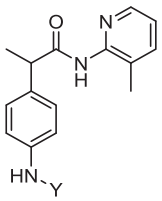

Compound	Y	Max inhibition (%)	IC_{50} (μM)	pIC_{50}±s.e.m[a]
TPA28	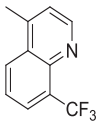	100	27	4.56 ± 0.04
TPA29	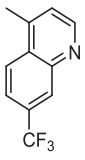	100	3.1	5.51 ± 0.03

[a] pI_{50} values (i.e.,-log10(IC_{50}) values) are indicated because the analysis method returns theseSE values, which are then antilogged to give the IC_{50} values for the inhibitable component (max inhibition) of the FAAH activity.

introduction of a methylene forced the methyl pyridine moiety partially outside the hydrophobic pocket toward the water filled cytosolic port (Supplementary data Fig. S6). Therefore, modifications altering the distance between the aromatic ring and the carbonyl should result in loss of activity by altering the proper positioning of this moiety. Moreover, this is consistent with the previous work that profenamides endowed with three-atom linker showed high FAAH inhibitory activity [11].

Role of the 3-methyl group on the pyridine ring. The importance of the 3-methyl group on pyridine ring was explored by comparing the inhibitory activity of **TPA1** and **TPA4** (Table 1).The presence of the 3-methyl substituent served to enhance activity by a factor of about 20 (**TPA4** IC_{50} 12.0 μM versus 0.59 μM for **TPA1**). Similarly, shifting the methyl group into position 5 (**TPA2**) or position 4 (**TPA3**) reduced the activity by 20- and 6-fold, respectively. This suggests a key role of the methyl group on the conformational behavior of **TPA1**, determining the relative positioning of the methyl-pyridine ring with respect to the amide bond, besides the specific apolar interactions formed by the methyl group with side chains of Val^{270} and Leu^{192}. To analyze further the effect of the methyl group, thermodynamic integration (TI) calculations [23] were used to calculate the differences in binding free energy between **TPA1** and **TPA4**. TI is best used in situations where small changes in structure correlate with relatively substantial changes in the binding affinity. Therefore, TI was used to elucidate the role of substitution of the methyl group on the pyridine ring in **TPA1** with the hydrogen group in **TPA4**. The calculation yielded a free energy difference of 1.0 kcal/mol, which would indicate a 5.7-fold higher affinity of **TPA1** versus **TPA4**, in good agreement with the experimental results.

Effect of modification of the pyridinamino moiety. The importance of the 2-pyridine ring was explored by comparing the inhibitory activity of **TPA4** with its analogues bearing different heterocyclic rings (Table 1). Substitution of the 2-pyridine moiety by a 3-pyridine (**TPA5**) resulted in about 2-fold increased activity (**TPA5**, IC_{50} 6.4 μM versus 12.0 μM of **TPA4**). Conversely the introduction of a 4-pyridine ring led to the poor FAAH inhibitor **TPA6**. On the other hand, replacement of the 2-pyridine ring of **TPA4** with pyrimidine (**TPA8**) improved the inhibitory potency (IC_{50} of 0.99 μM), while the change by pyrazine (**TPA9**) and quinoline (**TPA10**) led to more modest improvements. Finally, the replacement of pyridine nitrogen of **TPA1** with a carbon atom to give the phenyl analog **TPA7** (IC_{50} 0.74 μM) produced no significant difference in inhibitory activity. This reinforces the relevance of the 3-methyl group for FAAH inhibition. Overall, these results are in agreement with the A1 binding mode, where the pyridine ring is embedded in a hydrophobic environment.

Effect of the modification of the 3-methyl group on the pyridine ring. Taking into account that the best inhibitory activity was found for compounds bearing a 3-methyl substituent and the lipophilic nature of the binding pocket, the effect of replacing the methyl with other lipophilic groups was explored (Table 1). The replacement of the methyl group with a halogen atom and a trifluoromethyl group increased inhibitory activity as compared to **TPA1**; the trifluoromethyl substituted (**TPA13**) IC_{50} value was 0.33 μM, while those of bromine (**TPA11**) and iodine (**TPA12**) derivatives were 0.13 μM and 0.10 μM respectively. The activity remarkably increased in the chlorine analog (**TPA14**). This compound showed a tenfold enhanced activity as compared to **TPA1** (**TPA14** IC_{50} 0.058 μM versus 0.59 μM of **TPA1**).

Effect of replacing the methyl group on C-α to carbonyl group. Removal of the methyl group **(TPA22)** is detrimental for the inhibitory activity (Table 4).

However, insertion of a second methyl group on the same carbon atom (**TPA23**) slightly reduced the inhibitory activity with respect to **TPA1** (IC_{50} value 1.8 μM). Taken together these results indicated that the presence of a lipophilic group on C-α to the carbonyl group is necessary for the activity and that the relative position of methyl and aromatic ring is not a key requisite. A comparison of substituent effects revealed that the introduction of 3, 4, 5, and 6 atom rings on C-α led to compounds **TPA24**, **TPA25, TPA26** and **TPA 27** showing a progressive reduction in inhibitory activity correlated to ring size increase.

Effect of replacing 2-(trifluoromethyl)pyridine ring. The 8-trifluoromethylquinoline (**TPA28**) and 7-trifluoromethylquinoline (**TPA29**) analogs showed respectively 45- and 5- fold reduction in

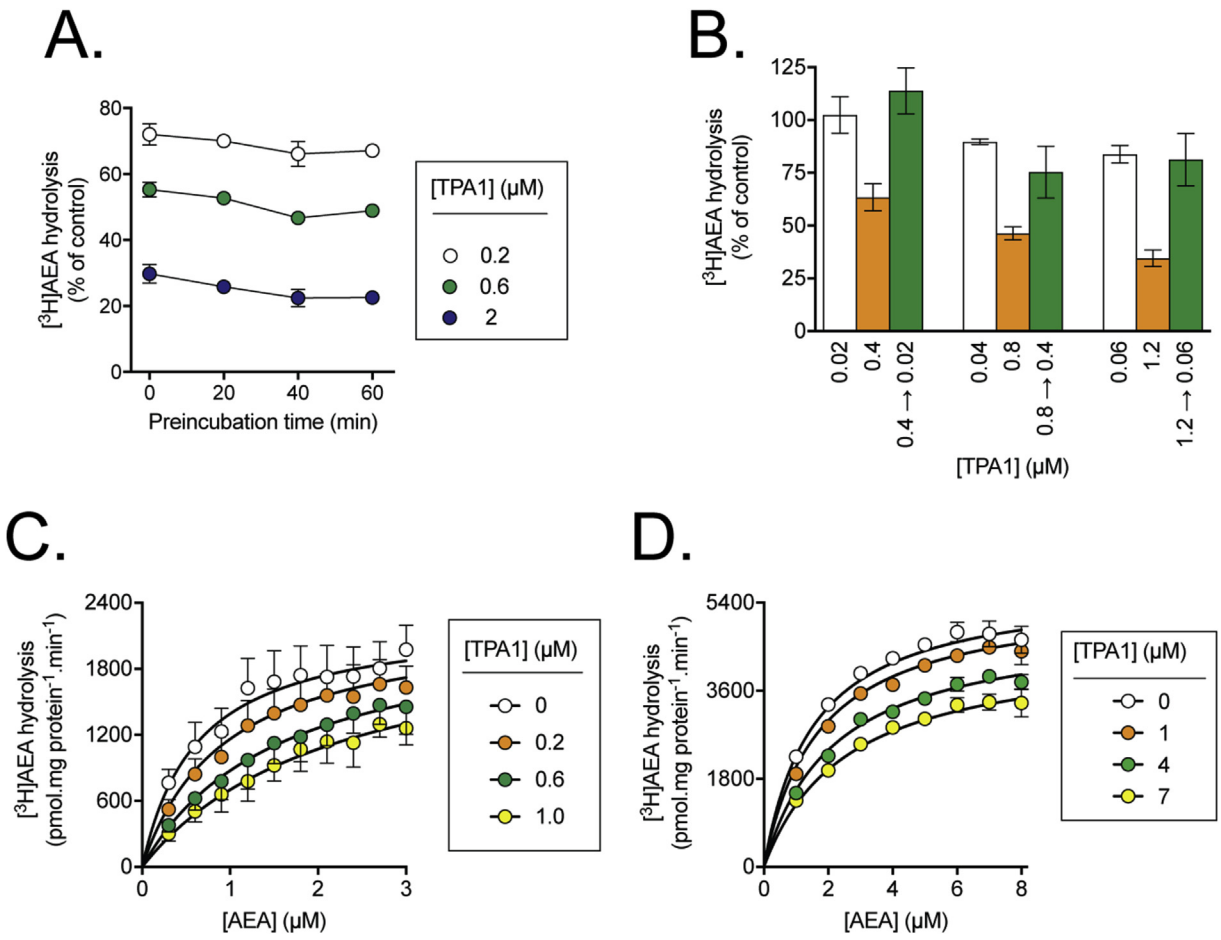

Fig. 2. Mode of inhibition of FAAH by **TPA1**. Panel A shows the time-dependency for rat. In Panel B, rat homogenates (at 20-fold normal strength) were preincubated with either vehicle, 0.4, 0.8 or 1.2 μM **TPA1** for 60 min. Aliquots were then diluted 20-fold and assayed for FAAH activity. These are shown as 0.4 → 0.02, 0.8 → 0.0.04 and 1.2 → 0.0.06. Concomitantly, **TPA1** was added to vehicle-preincubated aliquots to give concentrations of 0.02, 0.04 and 0.06 μM (representing free concentrations after a 20- fold dilution), 0.4, 0.8 and 1.2 μM final concentrations. The panel shows the data as % of corresponding control. Panel C shows the kinetics of the inhibition of rat FAAH. The data was better fitted by a competitive mode of inhibition (K_i value = 0.39 ± 0.03 μM) than by a mixed-type inhibition. Panel D shows the corresponding curves for inhibition of mouse FAAH. The data was better fitted by a mixed model inhibition (K_i = 6.3 ± 1.2 μM; α = 4.2 ± 1.6 [for a competitive inhibitor, α→∞; for a non-competitive inhibitor, α = 1]) than by a competitive mode of inhibition. All data are means ± SEM, n = 3–4.

inhibitory activity as compared to **TPA1** (Table 5). These results indicate that the presence of a larger aromatic system is detrimental for the activity, and that the presence of the 8-trifluoromethyl group in **TPA28**, which resembles the 2-trifluoromethyl group of **TPA1**, is relevant for the activity.

2.2.4. COX inhibitory activity

Among the novel compounds, **TPA1** and the most potent **TPA14** were chosen for further investigation. Given the ability of Ibu-AM5 and Flu-AM1 to inhibit COX [11,23], we investigated the ability of **TPA1** and **TPA14** to inhibit COX-1 and COX-2 (Fig. 4). Two substrates were investigated, arachidonic acid (AA, for both COX isoforms) and 2-acylglycerol (2-AG, for COX-2; COX-1 does not catalyze the cyclooxygenation of this compound). Flurbiprofen was used as positive control. In contrast to **Ibu-AM5** and **Flu-AM1**, **TPA1** showed a very weak COX-1 inhibition and did not inhibit COX-2 cyclooxygenation of either AA or 2-AG. A similar pattern of inhibition was seen with **TPA14** on COX-2, although this compound at a very high concentration (100 μM) produced a partial inhibition of COX-1. Thus, the structural modifications described in the present paper result in a loss of activity towards COX isoforms.

2.2.5. Mode of inhibition of FAAH by TPA14

Compound **TPA14** showed no time-dependent improvement of potency, indicating its reversible mechanism of action (Fig. 5A). This was confirmed by dilution experiments (Fig. 5B). The kinetics of inhibition were also investigated on rat and mouse FAAH. In the rat, **TPA14** inhibition of [^{3}H]AEA hydrolysis was better fitted by a non-competitive inhibition mode than by a mixed one, whereas in the mouse, **TPA14** showed a mixed-type inhibition of the hydrolysis.

2.2.6. Cross competition experiments

To investigate if **TPA1** and **TPA14** act in a mutually exclusive manner or in a cooperative manner, the two compounds were assayed together. The FAAH activity in the presence of different concentrations of both compounds was assessed and the data plotted per se in the left columns of Fig. 6 and as 1/v vs. the concentration of one of the compounds in the right columns. When compounds act as mutually exclusive inhibitors, the lines in the right columns should be parallel [25].

This is the case for **TPA1** and **TPA14** in both rat and mouse, suggesting that the compounds behave as mutually exclusive inhibitors. These data indicate that **TPA1** and **TPA14** act as FAAH inhibitors with different inhibition modes, suggesting that these

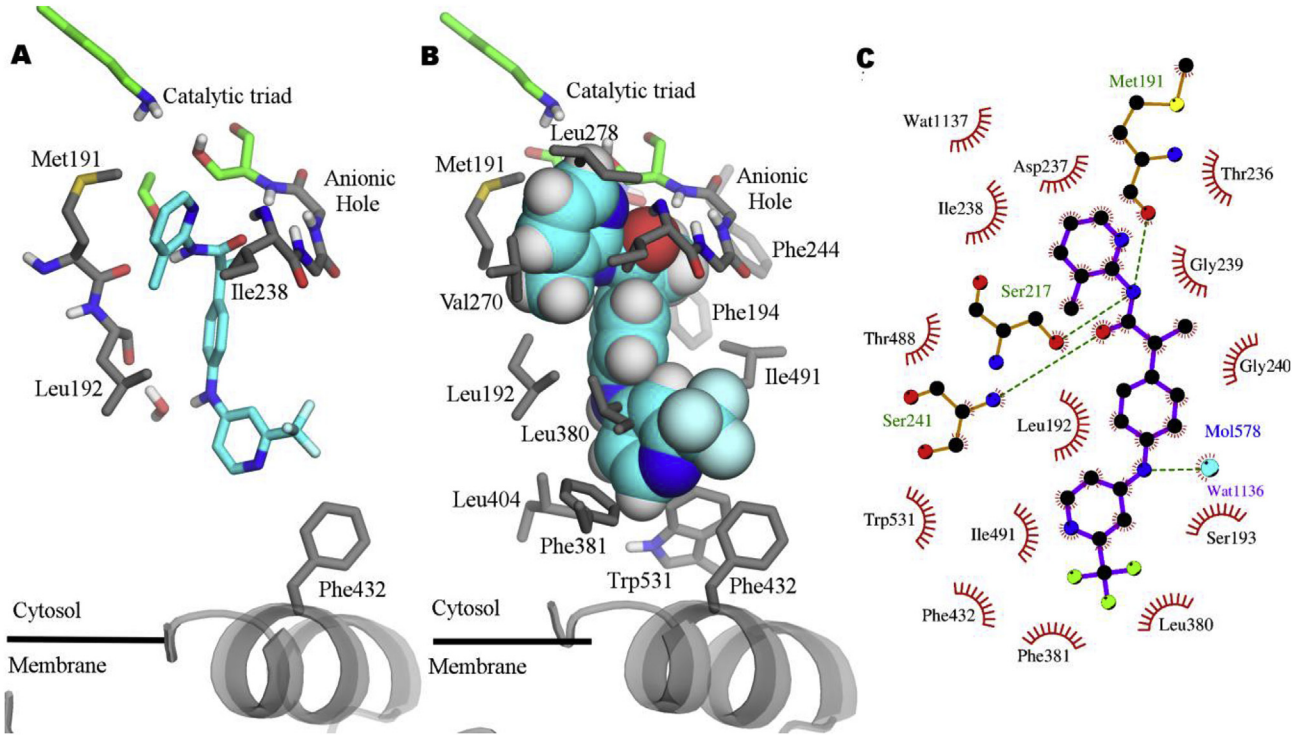

Fig. 3. A1-mode of **TPA1** refined after 100 ns of MD. A) Hydrogen bond of **TPA1** (cyan, in sticks) in A1-mode. B) Apolar interactions in the binding pocket of the FAAH. The ligand **TPA1** is represented in cyan by van der Waals spheres. C) LIGPLOT+ [22] interaction diagram. TPA1 (purple) and protein side chains (orange) are shown in ball-and-stick representation. Hydrogen bonds are shown as green dotted lines, spiked arcs represent apolar interactions. (For interpretation of the references to colour in this figure legend, the reader is referred to the web version of this article.)

structurally closely related compounds may involve distinct binding modes with the enzyme, presumably through either partial overlapping of the binding sites or conformational reshaping of the binding site.

In order to analyze the molecular basis of these subtle effects, we used TI calculations, to carry out the alchemical mutation from methyl (**TPA1**) to bromine (**TPA11**), trifluoromethyl (**TPA13**) or chlorine (**TPA14**). TI calculations showed that only the trifluoromethyl substitution increased the affinity in the A1-mode ($\Delta\Delta G = -0.83$ kcal/mol), while both bromine and chlorine substitutions resulted in a slight detrimental effect on the binding free energy (0.2 and 0.3 kcal/mol, respectively). These latter results were in contrast with the observed activities of **TPA11** and **TPA14** (0.13 μM and 0.058 μM, respectively), suggesting that for halogenated derivatives, the binding is different (albeit mutually exclusive) from the A1-mode described for **TPA1**. The simplest explanation is that there are two binding modes for the compounds, one competitive and another non-competitive, and that the compounds show different affinities for the two sites. The different potencies and different inhibition kinetics determined in rat and mouse FAAH (Figs. 2 and 5) suggest that the modestly different structures of these enzymes (Supplementary data Figs. S7 and S8) are sufficient to alter the relative affinities (and hence mode of inhibition) of the two sites towards the compounds. Moreover, we found a similar behavior for **IbuAM5** and **FluAM1**, lower potencies in mouse FAAH and different inhibition modes. Further experiments are required to clarify the molecular mechanism of inhibition.

3. Conclusions

In the present study by replacement of **Ibu-AM5** isobutyl chain with a trifluoromethylamino moiety led to a novel class of FAAH inhibitors. The *N*-(heteroaryl)-2-(4-((2-(trifluoromethyl)pyridin-4-yl)amino)phenyl)propanamides were found to act as reversible inhibitors. The 2-amino-3-methylpyridine amide (**TPA1**) retained the FAAH inhibitory potency of Ibu-AM5 and behaved essentially as competitive inhibitor in the rat enzyme. Docking and MD studies indicated the acyl chain binding (ABP) channel in proximity to the catalytic triad is the preferential **TPA1** binding site. Structure-activity relationship studies indicated that the FAAH inhibitory activity was enhanced by the presence of 3-substituted pyridinamide moiety. The 2-amino-3-chloropyridine amide (**TPA14**) was the most potent analogue in this series and behaved essentially as non-competitive inhibitor in the rat.

4. Experimental section

4.1. Chemistry

4.1.1. General methods

Commercially available solvents and reagents were used without further purification unless otherwise stated. Tetrahydrofuran (THF) was freshly distilled from sodium/benzophenone. Reactions requiring anhydrous conditions were performed in oven-dried glassware under argon atmosphere. ^{1}H NMR spectra were recorded on a Varian Inova 500 spectrometer. The chemical shifts (δ) are reported in part per million downfield from tetramethylsilane (TMS), which was used as internal standard, and the spectra were recorded in DMSO-d_6. Splitting patterns are designated as singlet (s), doublet (d), triplet (t), quartet (q), and multiplet (m). Infrared spectra were recorded on a Bruker Vector 22 spectrometer. The main bands are given in cm^{-1}. Melting points (m.p.) were determined on a Stuart Scientific Melting point SMP1 apparatus

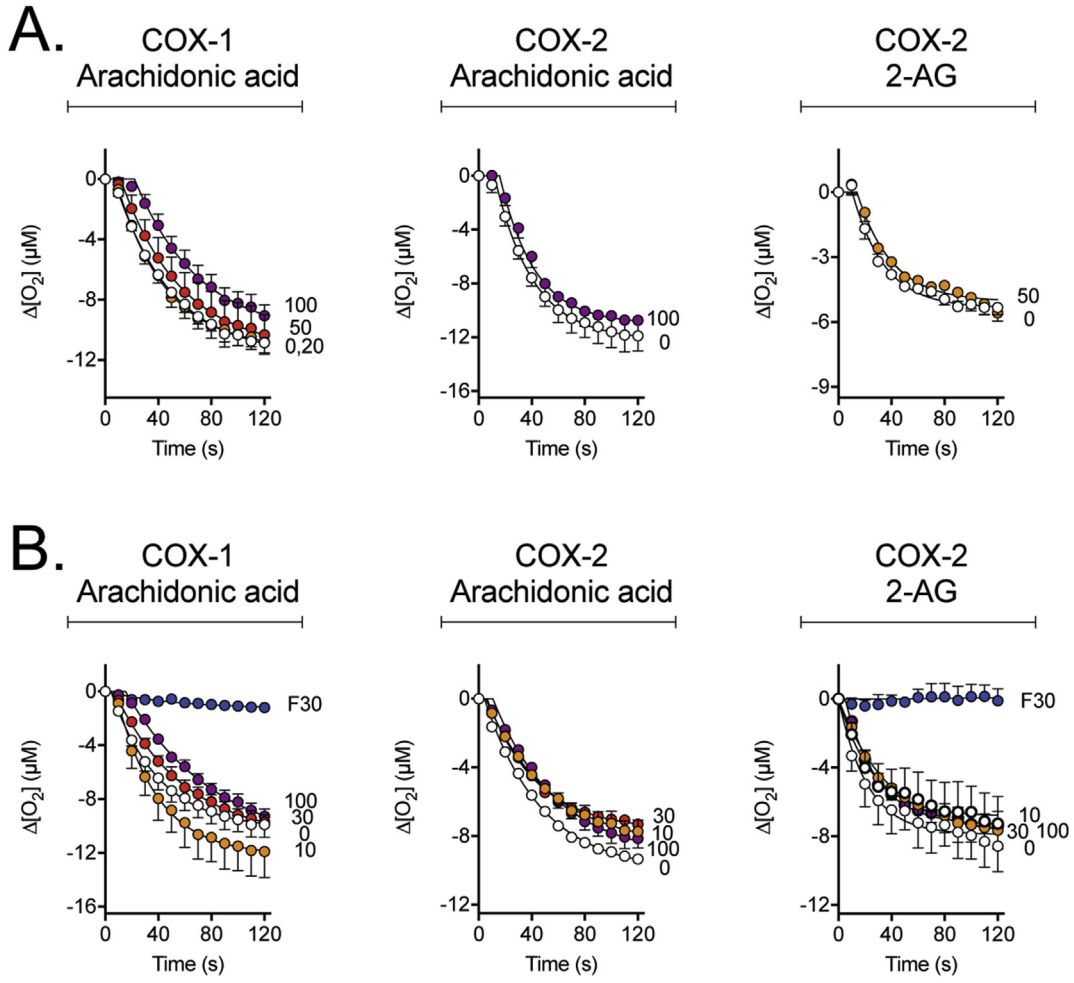

Fig. 4. Effects of A, **TPA1** and B, **TPA14** upon the cyclooxygenation of 10 μM arachidonic acid or 2-AG by COX-1 and -2. Shown are means ± SEM, n = 3–4 for the changes in oxygen tension following addition of enzyme in the presence of the compounds. The concentrations, in μM, of the compounds are shown on the right of each panel (F30 refers to 30 μM flurbiprofen, used as a positive control). The enzyme isoform and substrate used is given above each panel. COX-1 does not metabolise 2-AG.

and are uncorrected. The purity of tested compounds was determined by combustion elemental analyses conducted by the Microanalytical Laboratory of the Chemistry Department of the University of Ferrara with a Yanagimoto MT-5 CHN recorder elemental analyzer and all values were within 0.4% of the calculated values, which indicates >95% purity of the tested compounds. Analytical thin layer chromatography was performed using 0.25 mm silica gel 60-F plates. Flash chromatography was performed using 200–400 mesh silica gel (Merk KGaA). Unless otherwise stated, yields refer to chromatography and spectroscopically pure materials.

*4.1.2. Methyl 2-(4-aminophenyl)propanoate (**2**)*

A solution of 2-(4-nitrophenyl)propanoic acid (**1**) (5 g, 26 mmol) in methanol (MeOH) (25 mL) was treated at room temperature with 37% aqueous hydrochloric acid (HCl) (1 mL) and then refluxed for 4 h. The solvent was removed under vacuum and crude methyl ester was used for the further step. Iron powder (14 g, 256 mmol) was suspended in a mixture of MeCN (50 mL) and water (4 mL); the mixture was treated with 37% HCl (0.1 mL), than refluxed for 1 h. After cooling at room temperature a solution of crude methyl ester in MeOH (5 mL) was added dropwise in 30 min and the resulting solution was refluxed overnight. The hot suspension was filtered on a celite pad and the filtrate evaporated to afford an orange oil that was dissolved in CH_2Cl_2 (40 mL) and extracted with a saturated $NaHCO_3$ aqueous solution (3 × 35 mL), dried over anhydrous Na_2SO_4 and evaporated under vacuum to give the methyl-2-(4-aminophenyl)propanoate **(2)** as orange oil. Yield 75%.^{1}H NMR (DMSO-d_6) δ 1.45 (d, J = 7.0 Hz, 3H), 3.60 (s, 3H), 3.75 (s, 2H), 3.80 (m, 1H), 6.65 (d, J = 7.0 Hz, 2H), 7.05 (d, J = 7.0 Hz, 2H). IR (Film) 3458, 3374, 2979, 2951, 1729, 1626 cm^{-1}. Anal. Calcd. for $C_{10}H_{13}NO_2$ (179.21): C, 67.02; H, 7.31; N, 7.82. Found: C, 67.08; H, 7.32; N, 7.85.

*4.1.3. Methyl (E)-2-(4-((5,5,5-trifluoro-4-oxopent-2-en-2-yl) amino)phenyl)propanoate (**4**)*

A mixture of methyl ester **2** (1.79 g, 10 mmol), and enol ether **3** (2.52 g, 15 mmol) in anhydrous MeCN (10 mL) was refluxed for 2 h. After cooling, the formed precipitate was collected by filtration, washed with di-isopropyl ether (iPr_2O), dried, and used without further purification. Yield 78%. Mp 43–45 °C. ^{1}H NMR (DMSO-d_6) δ 1.45 (d, J = 5.0 Hz, 3H), 2.24 (s, 3H), 3.70 (s, 3H), 3.98 (m, 1H), 5.74 (s, 1H), 6.94 (d, J = 8.4 Hz, 2H), 7.73 (d, J = 8.4 Hz, 2H), 12.48 (s, 1H). IR (Nujol) 3376, 2981, 2936, 1729 cm^{-1}. Anal. Calcd. for $C_{15}H_{16}F_3NO_3$ (315.29): C, 57.14; H, 5.12; N, 4.44. Found: C, 57.18; H, 5.13; N, 4.46.

*4.1.4. Methyl 2-(4-(((1E,3E)-1-(dimethylamino)-6,6,6-trifluoro-5-oxohexa-1,3-dien-3-yl)amino)phenyl)propanoate (**5**)*

A mixture of **4** (1.58 g, 5 mmol), and DMF-DMA (1.79 g, 15 mmol)

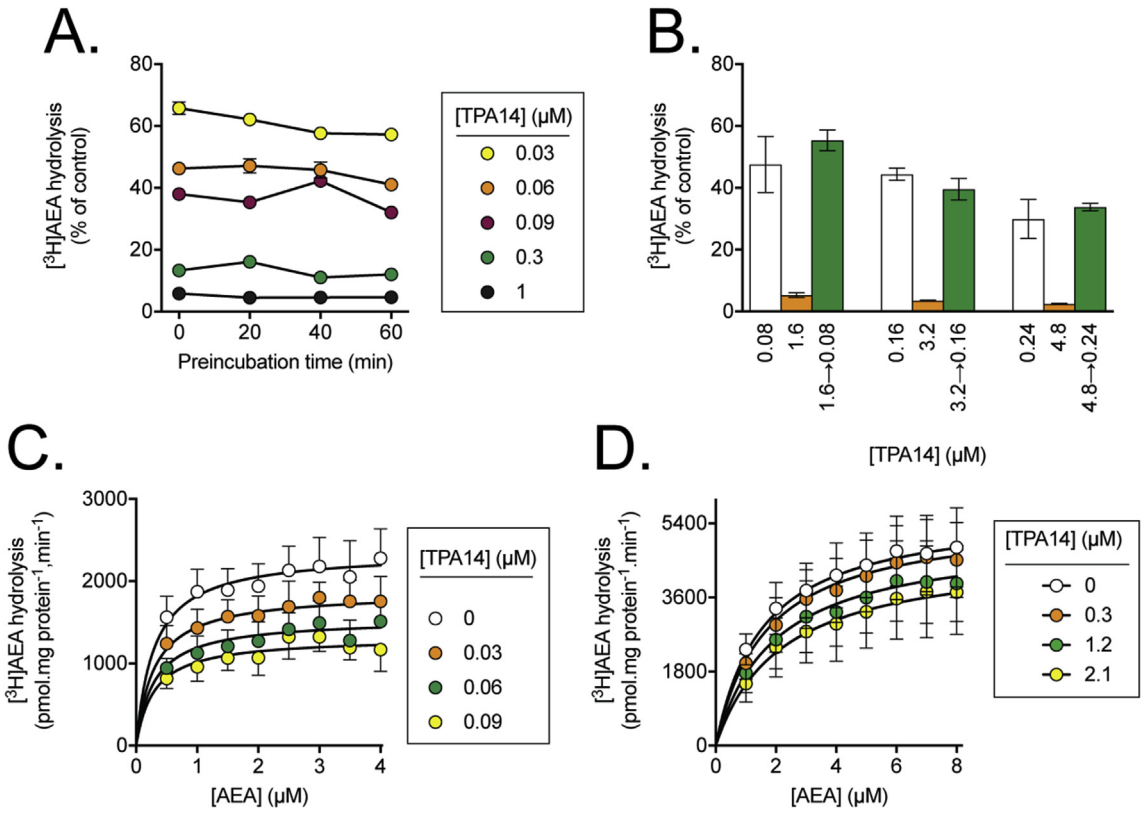

Fig. 5. Mode of inhibition of FAAH by **TPA14**. Panel A shows the time-dependency for rat. In Panel B, rat homogenates (at 20-fold normal strength) were preincubated with either vehicle, 1.6, 3.2 or 4.8 μM TPA14 for 60 min. Aliquots were then diluted 20-fold and assayed for FAAH activity. These are shown as 1.6 → 0.08 etc. Concomitantly, **TPA14** was added to vehicle-preincubated aliquots to give concentrations of 0.08, 0.16 and 0.24 μM (representing free concentrations after a 20- fold dilution), 1.6, 3.2 and 4.8 μM final concentrations. The panel shows the data as % of corresponding control. Panel C shows the kinetics of the inhibition of rat FAAH. The data was better fitted by a non-competitive mode of inhibition (K_i value = 0.11 ± 0.0017 μM) than by a mixed-type inhibition. Panel D shows the corresponding curves for inhibition of mouse FAAH. The data was better fitted by a mixed model inhibition (K_i = 3.0 ± 0.65 μM; α 3.2 ± 1.3) than by a competitive mode of inhibition. All data are means ± SEM, n = 3.

in anhydrous toluene (20 mL) was refluxed for 1 h, then was allowed to reach the room temperature and stirred for additional 24 h. The mixture was carefully concentrated in vacuum to give **5**. Yield 88%. Oil. ^{1}H NMR (DMSO-d_6) δ 1.41 (d, J = 6.5 Hz, 3H), 2.75 (s, 3H), 3.10 (s, 3H), 3.60 (s, 3H), 3.85 (m, 1H), 4.98 (d, J = 10.5 Hz, 1H), 5.74 (s, 1H), 7.25 (d, J = 7.5 Hz, 2H), 7.33 (d, J = 7.5 Hz, 2H), 7.91 (d, J = 10.5 Hz, 1H), 12.76 (s, 1H). IR (Film) 1722, 1671 cm^{-1}. Anal. Calcd. for $C_{18}H_{21}F_3N_2O_3$ (370.37): C, 58.37; H, 5.72; N, 7.56. Found: C, 58.42; H, 5.73; N, 7.53.

4.1.5. Methyl 2-(4-((2-(trifluoromethyl)pyridin-4-yl)amino)phenyl) propanoate (**6**)

To a solution of **5** (0.74 g, 2 mmol) in dry DMF (5 mL), ammonium acetate (0.31 g, 4 mmol) was added and the mixture was gently refluxed for 1.5 h. The mixture was carefully concentrated in vacuum, and then ice-water (15 mL) was added. The formed solid was filtered off, washed with water, air-dried, and then recrystallized with iPr_2O to give **6**. Yield 75%. Mp 36–39 °C. ^{1}H NMR (DMSO-d_6) δ 1.57 (d, J = 6.5 Hz, 3H), 3.92 (m, 1H), 3.98 (s, 3H), 6.50 (m, 2H), 6.75 (m, 2H), 7.02 (m, 2H), 8.48 (m, 1H), 9.69 (s, 1H). IR (Nujol) 3346, 3312, 1737, 1670 cm^{-1}. Anal. Calcd. for $C_{16}H_{15}F_3N_2O_2$ (324.30): C, 59.26; H, 4.66; N, 8.64. Found: C, 59.33; H, 4.65; N, 8.67.

4.1.6. 2-(4-((2-(Trifluoromethyl)pyridin-4-yl)amino)phenyl) propanoic acid (**7**)

To a solution of the ester **6** (0.65 g; 2 mmol) in EtOH (20 mL) 5 N solution of NaOH (4 mL) and water (4 mL) were added. The resulting mixture was stirred at r.t. for 24 h. After removing EtOH under vacuum, ice was added to the residue and then acidified with aqueous 20% HCl solution until pH 3-4. The formed precipitate was filtered, washed with water and re-crystallized with EtOH to obtain the title compound. Yield 69%. Mp 37–39 °C. ^{1}H NMR (DMSO-d_6) δ 1.37 (d, J = 7.0 Hz, 3H), 3.67 (q, J = 7.0 Hz, 1H), 7.08 (m, 1H), 7.20 (m, 3H), 7.30 (m, 2H), 8.30 (m, 1H), 9.22 (s, 1H), 12.28 (s, 1H). IR (Nujol) 3336, 3296, 2485, 1683, 1603 cm^{-1}. Anal. Calcd. for $C_{15}H_{13}F_3N_2O_2$ (320.27): C, 58.07; H, 4.22; N, 9.03. Found: C, 58.12; H, 4.21; N, 9.06.

4.1.7. General procedure for the synthesis of amides ***TPA1-29***

A solution of acids **7, 9, 14, 21, 42-45** (1 mmol), EDC (0.19 g, 1.1 mmol) and HOBt (0.13 g, 1 mmol) in anhydrous MeCN (10 mL) was stirred at r.t. for 30 min, then the appropriate amine (1 mmol) was added. The mixture was stirred at r.t. for 12 h in the case of aliphatic amines and 36 h in the case of heteroaromatic and aromatic amines. After the solvent was removed under vacuum. The residue was dissolved in ethyl acetate (AcOEt) (20 mL) and washed sequentially with brine (2 × 5 mL), 10% citric acid (2 × 5 mL), saturated $NaHCO_3$ aqueous solution (2 × 5 mL) and water (2 × 5 mL). The organic layer was dried over anhydrous Na_2SO_4 and evaporated under vacuum to give the title amides.

*4.1.7.1. N-(3-Methylpyridin-2-yl)-2-(4-((2-(trifluoromethyl)pyridin-4-yl)amino)phenyl)propanamide (**TPA1**).* Obtained following the general procedure by the condensation between **7** and 2-amino-3-methylpyridine. Yield 79%. M p 109–110 °C. ^{1}H NMR (DMSO-d_6) δ 1.15 (d, J = 6.2 Hz, 3H), 1.50 (s, 3H), 3.79 (q, J = 6.2 Hz, 1H),

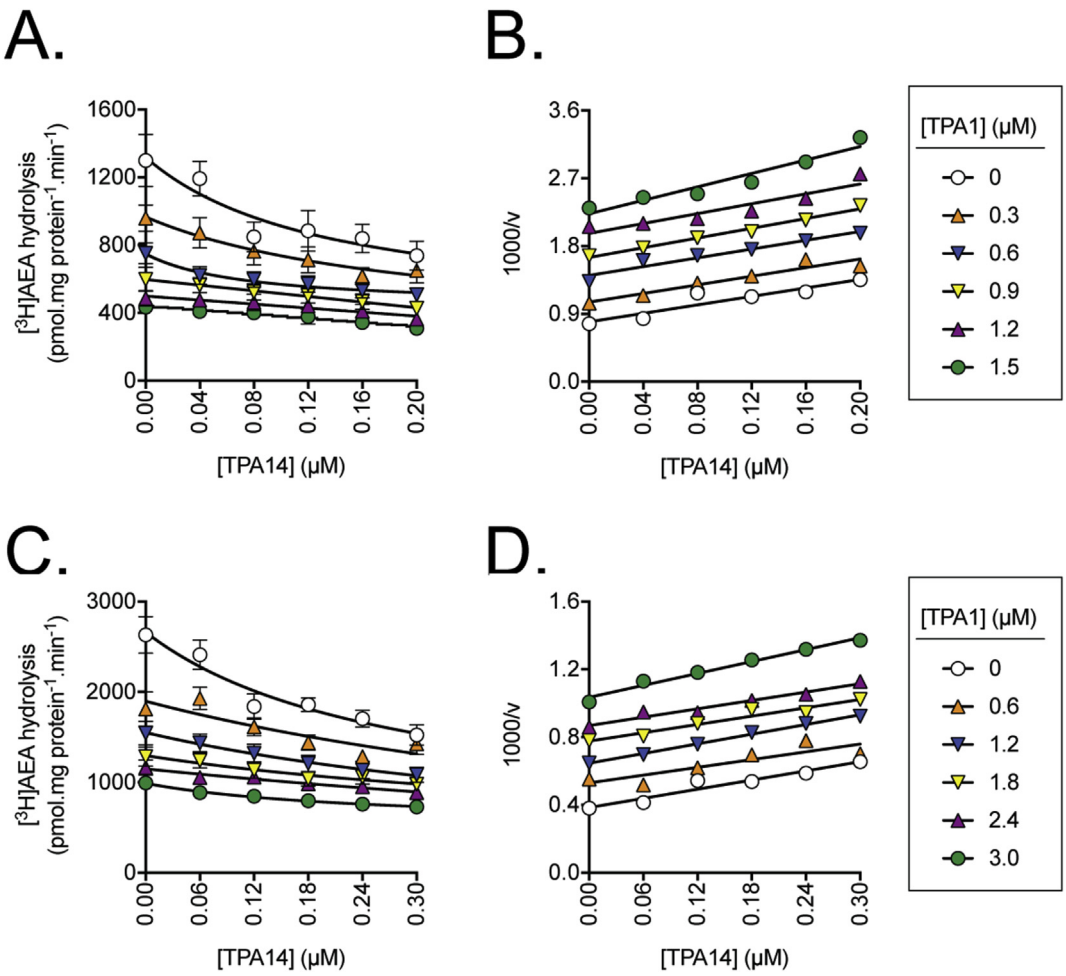

Fig. 6. Multiple-inhibitor experiments for the inhibition of A, B rat brain and C, D mouse brain [^{3}H]AEA (0.5 μM) hydrolysis using **TPA1** and **TPA14**. The left panels show the untransformed data and are means ± SEM, N = 6. The right panels show the Dixon plots of the mean data.

7.18–7.53 (m, 8H), 8.40 (m, 2H), 9.28 (s, 1H), 10.26 (s, 1H). ^{13}C NMR (DMSO-d_6) δ 25.3, 26.1, 52.2, 110.0, 113.5, 117.9, 129.1, 136.1, 136.2, 144.4, 145.8, 155.5, 155.8, 157.7, 159.8, 183.4. IR (Nujol) 1674, 1620, 1603 cm^{-1}. Anal. Calcd. for $C_{21}H_{19}F_3N_4O$ (400.40): C, 62.99; H, 4.78; N, 13.99. Found: C, 62.94; H, 4.79; N, 14.02.

*4.1.7.2. N-(5-methylpyridin-2-yl)-2-(4-((2-(trifluoromethyl)pyridin-4-yl)amino)phenyl)propanamide (**TPA2**).* Obtained following the general procedure by the condensation between **7** and 2-amino-5-methylpyridine. Yield 25%. M p 148–150 °C. ^{1}H NMR (DMSO-d_6) δ 1.46 (m, 3H), 2.64 (s, 3H), 3.90 (m, 1H), 7.19–7.69 (m, 9H), 8.39 (m, 1H), 9.39 (s, 1H). ^{13}C NMR (DMSO-d_6) δ 25.3, 27.4, 52.2, 110.0, 113.5, 117.9, 129.1, 136.2, 137.0, 145.9, 153.2, 155.5, 157.7, 158.3, 159.7, 183.2. IR (Nujol) 1666, 1601 cm^{-1}. Anal. Calcd. for $C_{23}H_{22}F_3N_5O_2$ (457.45): C, 60.39; H, 4.85; N, 15.31. Found: C, 60.33; H, 4.84; N, 15.35.

*4.1.7.3. N-(4-Methylpyridin-2-yl)-2-(4-((2-(trifluoromethyl)pyridin-4-yl)amino)phenyl)propanamide (**TPA3**).* Obtained following the general procedure by the condensation between **7** and 2-amino-4-methylpyridine. Yield 31%. M p 53–55 °C. ^{1}H NMR (DMSO-d_6) δ 1.47 (m, 3H), 2.65 (s, 3H), 3.94 (m, 1H), 7.06–7.56 (m, 9H), 8.40 (m, 1H), 9.40 (s, 1H). ^{13}C NMR (DMSO-d_6) δ 25.3, 27.3, 52.1, 110.0, 113.6, 117.9, 120.3, 136.1, 144.4, 146.0, 155.7, 155.8, 156.2, 158.1, 159.7, 179.8. IR (Nujol) 2923, 1681, 1601 cm^{-1}. Anal. Calcd. for $C_{23}H_{22}F_3N_5O_2$ (400.40): C, 62.99; H, 4.78; N, 13.99. Found: C, 63.06; H, 4.79; N, 13.95.

*4.1.7.4. N-(pyridin-2-yl)-2-(4-((2-(trifluoromethyl)pyridin-4-yl)amino)phenyl)propanamide (**TPA4**).* Obtained following the general procedure by the condensation between **7** and 2-aminopyridine. Yield 30%. M p 133–135 °C. ^{1}H NMR (DMSO-d_6) δ 1.14 (m, 3H), 4.22 (m, 1H), 7.18–7.84 (m, 10H), 8.39 (m, 1H), 9.34 (s, 1H). ^{13}C NMR (DMSO-d_6) δ 25.3, 52.2, 109.8, 113.7, 115.8, 117.6, 122.3, 130.0, 136.0, 136.2, 145.6, 155.8, 157.9, 159.5, 182.9. IR (Nujol) 3298, 2924, 1668, 1602 cm^{-1}. Anal. Calcd. for $C_{20}H_{17}F_3N_4O$ (386.37): C, 62.17; H, 4.43; N, 14.50. Found: C, 62.22; H, 4.42; N, 14.53.

*4.1.7.5. N-(pyridin-3-yl)-2-(4-((2-(trifluoromethyl)pyridin-4-yl)amino)phenyl)propanamide (**TPA5**).* Obtained following the general procedure by the condensation between **7** and 3-aminopyridine. Yield 44%. M p 156–158 °C. ^{1}H NMR (DMSO-d_6) δ 1.44 (m, 3H), 3.99 (m, 1H), 7.13–8.33 (m, 11H). ^{13}C NMR (DMSO-d_6) δ 25.3, 52.2, 110.0, 113.6, 117.7, 121.4, 130.0, 135.9, 136.2, 140.9, 141.4, 144.0, 145.7, 158.0, 159.3, 182.7. IR (Nujol) 3274, 2955, 1695, 1603 cm^{-1}. Anal. Calcd. for $C_{20}H_{17}F_3N_4O$ (386.37): C, 62.17; H, 4.43; N, 14.50. Found: C, 62.12; H, 4.41; N, 14.48.

*4.1.7.6. N-(pyridin-4-yl)-2-(4-((2-(trifluoromethyl)pyridin-4-yl)amino)phenyl)propanamide (**TPA6**).* Obtained following the general procedure by the condensation between **7** and 4-aminopyridine. Yield 22%. M p 128–130 °C. ^{1}H NMR (DMSO-d_6) δ 1.15 (d, J = 5.5 Hz, 3H), 3.61 (q, J = 5.5 Hz, 1H), 7.06 (m, 2H), 7.19 (m, 4H), 7.31 (m, 2H), 7.57 (m, 1H), 8.28 (m, 2H), 9.24 (s, 1H), 10.54 (s, 1H). ^{13}C NMR

(DMSO-d_6) δ 25.3, 52.3, 109.8, 112.3, 113.1, 118.0, 130.0, 134.2, 136.1, 141.3, 114.9, 152.4, 155.6, 158.1, 159.1, 181.9. IR (Nujol) 1602, 1515 cm^{-1}. Anal. Calcd. for $C_{20}H_{17}F_3N_4O$ (386.37): C, 62.17; H, 4.43; N, 14.50. Found: C, 62.12; H, 4.44; N, 14.48.

*4.1.7.7. N-(o-tolyl)-2-(4-((2-(trifluoromethyl)pyridin-4-yl)amino) phenyl)propanamide (**TPA7**).* Obtained following the general procedure by the condensation between **7** and 2-methylaniline. Yield 60%. M p 212–214 °C. ^{1}H NMR (DMSO-d_6) δ 1.03 (d, J = 6.0 Hz, 3H), 2.08 (s, 3H), 3.92 (q, J = 7.0 Hz, 1H), 7.07 (m, 2H), 7.13–7.23 (m, 5H), 7.32 (m, 1H), 7.44 (m, 2H), 8.29 (m, 1H), 9.22 (s, 1H), 9.38 (s, 1H). ^{13}C NMR (DMSO-d_6) δ 19.8, 25.3, 52.2, 109.9, 112.0, 117.9, 126.7, 129.8, 130.4, 136.2, 139.8, 145.8, 155.5, 157.6, 159.7, 180.9. IR (Nujol) 1667, 1604 cm^{-1}. Anal. Calcd. for $C_{22}H_{20}F_3N_3O$ (399.40): C, 66.16; H, 5.05; N, 10.52. Found: C, 66.22; H, 5.03; N, 10.55.

*4.1.7.8. N-(pyrimidin-2-yl)-2-(4-((2-(trifluoromethyl)pyridin-4-yl) amino)phenyl)propanamide (**TPA8**).* Obtained following the general procedure by the condensation between **7** and 2-aminopyrimidine. Yield 31%. mp 98–100 °C. ^{1}H NMR (DMSO-d_6) δ 1.40 (d, J = 7.0 Hz, 3H), 4.10 (q, J = 7.0 Hz, 1H), 7.17 (m, 1H), 7.20 (m, 4H), 7.40 (m, 2H), 8.28 (m, 1H), 8.64 (m, 2H), 9.21 (s, 1H), 10.71 (s, 1H). ^{13}C NMR (DMSO-d_6) δ 25.2, 52.2, 109.7, 117.8, 125.9, 127.6, 136.0, 136.2, 144.6, 146.2, 154.2, 157.7, 158.7, 160.3, 183.0. IR (Nujol) 1701, 1602 cm^{-1}. Anal. Calcd. for $C_{19}H_{16}F_3N_5O$ (387.36): C, 58.91; H, 4.16; N, 18.08. Found: C, 58.96; H, 4.15; N, 18.05.

*4.1.7.9. N-(pyrazin-2-yl)-2-(4-((2-(trifluoromethyl)pyridin-4-yl) amino)phenyl)propanamide (**TPA9**).* Obtained following the general procedure by the condensation between **7** and 2-aminopyrazine. Yield 46%. mp 82–83 °C. ^{1}H NMR (DMSO-d_6) δ 1.44 (d, J = 7.0 Hz, 3H), 4.06 (q, J = 7.0 Hz, 1H), 7.07 (m, 1H), 7.21 (m, 3H), 7.32 (m, 1H), 7.43 (m, 2H), 8.32 (m, 2H), 9.22 (s, 1H), 9.34 (s, 1H), 10.95 (s, 1H). ^{13}C NMR (DMSO-d_6) δ 25.3, 52.2, 110.0, 117.9, 129.0, 136.0, 137.5, 144.1, 145.8, 150.5, 155.4, 157.7, 159.9, 183.5. IR (Nujol) 1701, 1602 cm^{-1}. Anal. Calcd. for $C_{19}H_{16}F_3N_5O$ (387.36): C, 58.91; H, 4.16; N, 18.08. Found: C, 58.87; H, 4.17; N, 18.11.

*4.1.7.10. N-(quinolin-8-yl)-2-(4-((2-(trifluoromethyl)pyridin-4-yl) amino)phenyl)propanamide (**TPA10**).* Obtained following the general procedure by the condensation between **7** and 8-aminoquinoline. Yield 69%. mp 185–187 °C. ^{1}H NMR (DMSO-d_6) δ 1.50 (d, J = 7.0 Hz, 3H), 3.57 (d, J = 7.0 Hz, 1H), 7.15 (d, J = 8.0 Hz, 4H), 7.57 (m, 5H), 8.26 (m, 1H), 8.37 (d, J = 8.5 Hz, 1H), 8.63 (d, J = 8.0 Hz, 1H), 8.85 (s, 1H), 9.21 (s, 1H). ^{13}C NMR (DMSO-d_6) δ 25.3, 52.2, 115.2, 117.8, 118.2, 123.4, 128.0, 129.2, 130.1, 136.1, 136.3, 137.2, 138.4, 144.4, 145.8, 150.2, 155.5, 157.6, 159.9, 183.3. IR (Nujol) 1657, 1600, 1523 cm^{-1}. Anal. Calcd. for $C_{24}H_{19}F_3N_4O$ (436.43): C, 66.05; H, 4.39; N, 12.84. Found: C, 66.10; H, 4.38; N, 12.81.

*4.1.7.11. N-(3-bromopyridin-2-yl)-2-(4-((2-(trifluoromethyl)pyridin-4-yl)amino)phenyl)propanamide (**TPA11**).* Obtained following the general procedure by the condensation between **7** and 2-amino-3-bromopyridine. Yield 77%. mp 199–201 °C. ^{1}H NMR (DMSO-d_6) δ 1.43 (d, J = 6.5 Hz, 3H), 3.88 (q, J = 6.5 Hz, 1H), 7.05 (m, 1H), 7.18 (d, J = 8.5 Hz, 2H), 7.22 (m, 2H), 7.41 (d, J = 8.0 Hz, 2H), 8.10 (m, 1H), 8.28 (m, 1H), 8.41 (m, 1H), 9.19 (s, 1H), 10.26 (s, 1H). ^{13}C NMR (DMSO-d_6) δ 26.1, 52.8, 113.3, 115.8, 129.4, 136.0, 136.5, 145.2, 145.6, 146.3, 153.9, 155.8, 158.1, 160.3, 180.1. IR (Nujol) 1670, 1603, 1532, 1462, 1377 cm^{-1}. Anal. Calcd. for $C_{20}H_{16}BrF_3N_4O$ (465.27): C, 51.63; H, 3.47; N, 12.04. Found: C, 51.58; H, 3.46; N, 12.07.

*4.1.7.12. N-(3-iodopyridin-2-yl)-2-(4-((2-(trifluoromethyl)pyridin-4-yl)amino)phenyl)propanamide (**TPA12**).* Obtained following the general procedure by the condensation between **7** and 2-amino-3-iodopyridine. Yield 33%. mp 210–211 °C. ^{1}H NMR (DMSO-d_6) δ 1.44 (d, J = 7.0 Hz, 3H), 3.88 (q, J = 7.5 Hz, 1H), 7.05 (m, 2H), 7.18 (m, 1H), 7.19 (d, J = 8.0 Hz, 2H), 7.41 (d, J = 8.5 Hz, 2H), 8.28 (m, 2H), 8.41 (m, 1H), 9.19 (s, 1H), 10.23 (s, 1H). ^{13}C NMR (DMSO-d_6) δ 26.2, 52.7, 90.3, 116.0, 129.4, 136.1, 136.5, 145.4, 145.8, 147.2, 153.9, 155.8, 158.1, 160.8, 181.3. IR (Nujol) 1667, 1602, 1531 cm^{-1}. Anal. Calcd. for $C_{20}H_{16}F_3IN_4O$ (512.27): C, 46.89; H, 3.15; N, 10.94. Found: C, 48.94; H, 3.16; N, 10.97.

*4.1.7.13. N-(3-(trifluoromethyl)pyridin-2-yl)-2-(4-((2-(trifluoromethyl)pyridin-4-yl)amino)phenyl)propanamide (**TPA13**).* Obtained following the general procedure by the condensation between **7** and 2-amino-3-(trifluoromethyl)pyridine. Yield 59%. Mp 188–190 °C. ^{1}H NMR (DMSO-d_6) δ 1.42 (d, J = 7.0 Hz, 3H), 3.91 (q, J = 7.0 Hz, 1H), 7.05 (m, 1H), 7.17 (s, 1H), 7.20 (d, J = 6.5 Hz, 2H), 7.39 (d, J = 7.0 Hz, 2H), 7.53 (m, 1H), 8.20 (m, 1H), 8.28 (m, 1H), 8.72 (m, 1H), 9.20 (s, 1H), 10.28 (s, 1H). ^{13}C NMR (DMSO-d_6) δ 26.2, 52.7, 116.8, 117.1, 120.3, 129.2, 136.3, 136.5, 142.9, 145.3, 145.9, 147.2, 155.8, 158.0, 160.9, 179.9. IR (Nujol) 1671, 1603 cm^{-1}. Anal. Calcd. for $C_{21}H_{16}F_6N_4O$ (454.37): C, 55.51; H, 3.55; N, 12.33. Found: C, 55.56; H, 3.56; N, 12.36.

*4.1.7.14. N-(3-Chloropyridin-2-yl)-2-(4-((2-(trifluoromethyl)pyridin-4-yl)amino)phenyl)propanamide (**TPA14**).* Obtained following the general procedure by the condensation between **7** and 2-amino-3-chloropyridine. Yield 78%. Mp 148–150 °C. ^{1}H NMR (DMSO-d_6) δ 1.44 (d, J = 5.5 Hz, 3H), 3.93 (q, J = 5.5 Hz, 1H), 7.07 (m, 1H), 7.21 (m, 3H), 7.32 (m, 1H), 7.41 (m, 2H), 7.96 (m, 1H), 8.29 (m, 1H), 8.38 (m, 1H), 9.22 (s, 1H), 10.32 (s, 1H). ^{13}C NMR (DMSO-d_6) δ 26.2, 52.8, 113.6, 117.8, 129.3, 136.2, 136.4, 145.2, 145.4, 146.0, 154.0, 155.8, 156.7, 160.5, 180.3. IR (Nujol) 1670, 1603 cm^{-1}. Anal. Calcd. for $C_{20}H_{16}ClF_3N_4O$ (420.81): C, 57.08; H, 3.83; N, 13.31. Found: C, 57.12; H, 3.84; N, 13.34.

*4.1.7.15. N-(pyridin-2-ylmethyl)-2-(4-((2-(trifluoromethyl)pyridin-4-yl)amino)phenyl)propanamide (**TPA15**).* Obtained following the general procedure by the condensation between **7** and 2-picolylamine. Yield 71%. Mp 73–75 °C. ^{1}H NMR (DMSO-d_6) δ 1.49 (m, 3H), 3.29 (m, 1H), 4.47 (s, 2H), 7.19–7.49 (m, 7H), 7.83 (m, 1H), 8.41 (m, 1H), 8.59 (m, 1H), 8.76 (m, 1H), 9.39 (s, 1H). ^{13}C NMR (DMSO-d_6) δ 25.2, 52.8, 54.0, 109.8, 113.5, 117.9, 120.3, 127.2, 129.0, 135.8, 136.0, 145.8, 146.2, 155.5, 157.7, 158.8, 159.6, 177.7. IR (Nujol) 2924, 1600, 1532 cm^{-1}. Anal. Calcd. for $C_{21}H_{19}F_3N_4O$ (400.40): C, 62.99; H, 4.78; N, 13.99. Found: C, 62.93; H, 4.80; N, 13.95.

*4.1.7.16. N-(pyridin-3-ylmethyl)-2-(4-((2-(trifluoromethyl)pyridin-4-yl)amino)phenyl)propanamide (**TPA16**).* Obtained following the general procedure by the condensation between **7** and 3-picolylamine. Yield 58%. Mp 143–145 °C. ^{1}H NMR (DMSO-d_6) δ 1.14 (m, 3H), 2.64 (s, 2H), 4.39 (m, 1H), 7.16–7.66 (m, 8H), 8.40–8.71 (m, 3H), 9.36 (s, 1H). ^{13}C NMR (DMSO-d_6) δ 25.2, 52.7, 53.7, 109.9, 113.5, 117.9, 127.2, 130.2, 135.9, 136.1, 145.8, 146.1, 148.2, 155.4, 155.5, 157.5, 159.6, 177.8. IR (Nujol) 2906, 1657, 1601 cm^{-1}. Anal. Calcd. for $C_{21}H_{19}F_3N_4O$ (400.40): C, 62.99; H, 4.78; N, 13.99. Found: C, 62.93; H, 4.77; N, 13.95.

*4.1.7.17. N-(2-((3-Methylpyridin-2-yl)amino)-2-oxoethyl)-2-(4-((2-(trifluoromethyl)pyridin-4-yl)amino)phenyl)propanamide (**TPA17**).* Obtained following the general procedure by the condensation between **9** and 2-amino-3-methylpyridine. Yield 76%. mp 228–230 °C. ^{1}H NMR (DMSO-d_6) δ 1.38 (m, 3H), 2.62 (s, 3H), 3.98 (m 3H), 7.19 (m, 2H), 7.30 (m, 2H), 7.46 (m, 2H), 7.53 (m, 2H), 8.36 (m, 1H), 8.53 (m, 1H). ^{13}C NMR (DMSO-d_6) δ 25.3, 26.2, 49.8, 52.2, 109.8, 113.3, 118.0, 129.1, 136.0, 136.1, 144.6, 145.8, 155.4, 155.7, 157.7, 159.9, 182.8. IR (Nujol) 1658, 1602 cm^{-1}. Anal. Calcd. for $C_{23}H_{22}F_3N_5O_2$

(457.45): C, 60.39; H, 4.85; N, 15.31. Found: C, 60.35; H, 4.60; N, 15.35.

*4.1.7.18. 1-(4-(3-Chlorophenyl)piperazin-1-yl)-2-(4-((2-(trifluoromethyl)pyridin-4-yl)amino)phenyl)propan-1-one (**TPA18**).* Obtained following the general procedure by the condensation between **7** and 1-(3-chlorophenyl)piperazine. Yield 67%. mp 78–80 °C. ^{1}H NMR (DMSO-d_6) δ 1.44 (d, J = 7.5 Hz, 3H), 2.66 (m, 1H), 2.99 (m, 1H), 3.18 (m, 2H), 3.59 (m, 4H), 4.16 (q, J = 7.0 Hz, 1H), 6.78 (m, 1H), 6.83 (m, 1H), 6.89 (m, 1H), 7.03 (m, 1H), 7.18 (m, 4H), 7.31 (m, 2H), 8.26 (m, 1H), 9.18 (s, 1H). ^{13}C NMR (DMSO-d_6) δ 25.6, 48.2, 50.8, 54.5, 110.1, 112.9, 114.1, 117.8, 123.0, 129.0, 132.8, 136.7, 136.4, 144.4, 145.8, 151.3, 155.4, 157.5, 159.8, 183.6. IR (Nujol) 1596, 1519 cm^{-1}. Anal. Calcd. for $C_{25}H_{24}ClF_3N_4O$ (488.93): C, 61.41; H, 4.95; N, 11.46. Found: C, 61.47; H, 4.94; N, 11.50.

*4.1.7.19. 1-(4-(4-Chlorophenyl)piperazin-1-yl)-2-(4-((2-(trifluoromethyl)pyridin-4-yl)amino)phenyl)propan-1-one (**TPA19**).* Obtained following the general procedure by the condensation between **7** and 1-(4-chlorophenyl)piperazine. Yield 82%. Mp 83–85 °C. ^{1}H NMR (DMSO-d_6) δ 1.32 (d, J = 6.5 Hz, 3H), 2.66 (m, 1H), 2.95 (m, 1H), 3.11 (m, 2H), 3.61 (m, 4H), 4.17 (q, J = 6.5 Hz, 1H), 6.89 (d, J = 8.0 Hz, 2H), 7.03 (m, 1H), 7.19 (m, 5H), 7.30 (d, J = 8.0 Hz, 2H), 8.27 (m, 1H), 9.18 (s, 1H). ^{13}C NMR (DMSO-d_6) δ 25.6, 48.2, 50.8, 54.5, 110.1, 117.8, 118.2, 130.3, 129.0, 136.4, 144.4, 145.8, 151.3, 155.4, 157.5, 159.8, 183.5. IR (Nujol) 1645, 1600 cm^{-1}. Anal. Calcd. for $C_{25}H_{24}ClF_3N_4O$ (488.93): C, 61.41; H, 4.95; N, 11.46. Found: C, 61.35; H, 4.93; N, 11.49.

*4.1.7.20. 1-(4-(2,3-Dimethylphenyl)piperazin-1-yl)-2-(4-((2-(trifluoromethyl)pyridin-4-yl)amino)phenyl)propan-1-one (**TPA20**).* Obtained following the general procedure by the condensation between **7** and 1-(2,3-dimethylphenyl)piperazine. Yield 62%. Mp 84–86 °C. ^{1}H NMR (DMSO-d_6) δ 1.33 (d, J = 6.0 Hz, 3H), 2.14 (s, 3H), 2.19 (s, 3H), 2.31 (m, 1H), 2.65 (m, 2H), 2.73 (m, 1H), 3.55 (m, 4H), 4.16 (q, J = 6.0 Hz, 1H), 6.74 (d, J = 7.5 Hz, 1H), 6.86 (d, J = 7.0 Hz, 1H), 6.98 (m, 1H), 7.05 (m, 1H), 7.19 (m, 3H), 7.31 (d, J = 8.0 Hz, 2H), 8.28 (m, 1H), 9.20 (s, 1H). ^{13}C NMR (DMSO-d_6) δ 20.2, 25.6, 28.7, 48.2, 50.8, 54.5, 109.8, 110.1, 118.2, 121.3, 122.4, 128.5, 129.0, 136.1, 139.0, 144.4, 145.8, 150.8, 155.4, 157.5, 159.8, 183.2. IR (Nujol) 3281, 2925, 1600 cm^{-1}. Anal. Calcd. for $C_{27}H_{29}F_3N_4O$ (482.54): C, 67.20; H, 6.06; N, 11.61. Found: C, 67.14; H, 6.04; N, 11.65.

*4.1.7.21. 1-(4-(o-Tolyl)piperazin-1-yl)-2-(4-((2-(trifluoromethyl)pyridin-4-yl)amino)phenyl)propan-1-one (**TPA21**).* Obtained following the general procedure by the condensation between **7** and 1-(2-methylphenyl)piperazine. Yield 68%. Mp 79–81 °C. ^{1}H NMR (DMSO-d_6) δ 1.33 (d, J = 6.5 Hz, 3H), 2.22 (s, 3H), 2.36 (m, 1H), 2.69 (m, 2H), 2.78 (m, 1H), 3.64 (m, 4H), 4.16 (q, J = 6.5 Hz, 1H), 6.87 (m, 1H), 6.94 (m, 1H), 7.15 (m, 5H), 7.31 (m, 1H), 7.31 (m, 2H), 8.28 (m, 1H), 9.21 (s, 1H). ^{13}C NMR (DMSO-d_6) δ 20.3, 25.6, 48.2, 50.8, 54.5, 110.1, 118.2, 120.7, 124.9, 128.6, 129.1, 13.4, 135.7, 136.2, 144.4, 145.8, 153.5, 155.5, 157.5, 159.7, 183.2. IR (Nujol) 3280, 1601, 1518, 1462 cm^{-1}. Anal. Calcd. for $C_{26}H_{27}F_3N_4O$ (468.51): C, 66.65; H, 5.81; N, 11.96. Found: C, 66.72; H, 5.82; N, 11.92.

*4.1.7.22. N-(3-Methylpyridin-2-yl)-2-(4-((2-(trifluoromethyl)pyridin-4-yl)amino)phenyl)acetamide (**TPA22**).* Obtained following the general procedure by the condensation between acid **14** and 2-amino-3-methylpyridine. Yield 78%. mp 138–140 °C. ^{1}H NMR (DMSO-d_6) δ 2.08 (s, 3H), 3.67 (s, 2H), 7.05 (m, 1H), 7.16 (m, 7H), 7.37 (m, 1H), 8.28 (m, 1H), 9.25 (s, 1H), 10.20 (s, 1H). ^{13}C NMR (DMSO-d_6) δ 25.8, 53.9, 110.0, 113.5, 117.9, 129.1, 136.1, 136.2, 144.4, 145.8, 155.5, 155.8, 157.7, 159.8, 179.9. IR (Nujol) 1602, 1518, 1462, 1377, 1180, 1135 cm^{-1}. Anal. Calcd. for $C_{20}H_{17}F_3N_4O$ (368.37): C, 62.17; H, 4.43; N, 14.50. Found: C, 62.22; H, 4.44; N, 11.53.

*4.1.7.23. 2-Methyl-N-(3-methylpyridin-2-yl)-2-(4-((2-(trifluoromethyl)pyridin-4-yl)amino)phenyl)propanamide (**TPA23**).* Obtained following the general procedure by the condensation between acid **21** and 2-amino-3-methylpyridine. Yield 61%. Mp 219–221 °C. ^{1}H NMR (DMSO-d_6) δ 1.60 (s, 6H), 2.06 (s, 3H), 7.09 (s, 1H), 7.23 (m, 4H), 7.46 (s, 2H), 7.64 (s, 1H), 8.24 (s, 1H), 8.30 (s, 1H), 9.24 (s, 1H). ^{13}C NMR (DMSO-d_6) δ 26.1, 28.1, 56.3, 110.0, 113.5, 117.9, 129.1, 136.1, 136.2, 144.4, 145.8, 155.5, 155.8, 157.7, 159.8, 187.2. IR (Nujol) 3290, 1661, 1605 cm^{-1}. Anal. Calcd. for $C_{22}H_{21}F_3N_4O$ (414.42): C, 63.76; H, 5.11; N, 13.52. Found: C, 63.71; H, 5.16; N, 13.57.

*4.1.7.24. N-(3-Methylpyridin-2-yl)-1-(4-((2-(trifluoromethyl)pyridin-4-yl)amino)phenyl)cyclopropane-1-carboxamide (**TPA24**).* Obtained following the general procedure by the condensation between acid **42** and 2-amino-3-methylpyridine. Yield 78%. Mp 209–211 °C. ^{1}H NMR (DMSO-d_6) δ 1.20 (m, 2H), 1.46 (m, 2H), 2.10 (s, 3H), 7.18 (m, 1H), 7.21 (m, 1H), 7.24 (m, 3H), 7.48 (m, 2H), 7.63 (m, 1H), 8.19 (s, 1H), 8.30 (m, 1H), 8.79 (s, 1H), 9.28 (s, 1H). ^{13}C NMR (DMSO-d_6) δ 19.2, 26.2, 30.9, 110.0, 113.5, 117.9, 121.9, 128.2, 134.7, 136.1, 144.4, 145.8, 153.7, 155.8, 157.7, 159.8, 182.3. IR (Nujol) 3401, 3244, 2924, 1688, 1599 cm^{-1}. Anal. Calcd. for $C_{22}H_{19}F_3N_4O$ (412.40): C, 64.07; H, 4.64; N, 13.59. Found: C, 64.01; H, 4.63; N, 13.55.

*4.1.7.25. N-(3-Methylpyridin-2-yl)-1-(4-((2-(trifluoromethyl)pyridin-4-yl)amino)phenyl)cyclobutane-1-carboxamide (**TPA25**).* Obtained following the general procedure by the condensation between acid **43** and 2-amino-3-methylpyridine. Yield 21%. Mp. 184–186 °C. ^{1}H NMR (DMSO-d_6) δ 1.83 (m, 2H), 1.98 (m, 4H), 2.88 (s, 3H), 7.06 (m, 1H), 7.19 (m, 2H), 7.22 (m, 2H), 7.47 (m, 2H), 7.61 (m, 1H), 8.21 (s, 1H), 8.30 (m, 1H), 9.22 (s, 1H), 9.70 (s, 1H). ^{13}C NMR (DMSO-d_6) δ 17.9, 26.2, 33.8, 54.3, 110.0, 113.5, 117.9, 122.7, 130.2, 136.1, 142.5, 145.8, 153.7, 155.8, 157.7, 159.8, 182.5. IR (Nujol) 3583, 2925, 1652, 1606, 1536 cm^{-1}. Anal. Calcd. for $C_{23}H_{21}F_3N_4O$ (426.43): C, 64.78; H, 4.96; N, 13.14. Found: C, 64.72; H, 4.95; N, 13.17.

*4.1.7.26. N-(3-Methylpyridin-2-yl)-1-(4-((2-(trifluoromethyl)pyridin-4-yl)amino)phenyl)cyclopentane-1-carboxamide (**TPA26**).* Obtained following the general procedure by the condensation between acid **44** and 2-amino-3-methylpyridine. Yield 27%. Mp 220 °C. ^{1}H NMR (DMSO-d_6) δ 1.69 (m, 4H), 1.92 (m, 4H), 2.72 (s, 3H), 7.05 (m, 1H), 7.20 (m, 4H), 7.46 (m, 2H), 7.58 (m, 1H), 8.19 (s, 1H), 8.27 (m, 1H), 9.22 (s, 1H), 9.51 (s, 1H). ^{13}C NMR (DMSO-d_6) δ 25.3, 26.2, 41.3, 54.2, 109.8, 113.5, 117.8, 122.6, 130.2, 136.0, 142.4, 145.7, 154.0, 155.8, 157.5, 159.7, 181.6. IR (Nujol) 3583, 3201, 2926, 1650, 1607 cm^{-1}. Anal. Calcd. for $C_{24}H_{23}F_3N_4O$ (440.46): C, 65.44; H, 5.26; N, 12.72. Found: C, 65.38; H, 5.24; N, 12.76.

*4.1.7.27. N-(3-Methylpyridin-2-yl)-1-(4-((2-(trifluoromethyl)pyridin-4-yl)amino)phenyl)cyclohexane-1-carboxamide (**TPA27**).* Obtained following the general procedure by the condensation between acid **45** and 2-amino-3-methylpyridine. Yield 55%. Mp. >250 °C. ^{1}H NMR (DMSO-d_6) δ 1.53 (m, 1H), 1.68 (m, 1H), 1.70–1.75 (m, 6H), 1.97 (s, 3H), 2.59 (m, 2H), 7.07–7.24 (m, 5H), 7.49 (m, 2H), 7.62 (m, 1H), 8.20 (s, 1H), 8.27 (m, 1H), 9.45 (s, 1H), 9.47 (s, 1H). ^{13}C NMR (DMSO-d_6) δ 21.3, 26.2, 27.3, 48.6, 109.9, 113.5, 117.9, 122.5, 130.2, 136.0, 142.3, 145.7, 154.0, 155.8, 157.5, 159.7, 182.0. IR (Nujol) 3583, 3288, 2925, 1645, 1606 cm^{-1}. Anal. Calcd. for $C_{25}H_{25}F_3N_4O$ (454.48): C, 66.07; H, 5.54; N, 12.33. Found: C, 66.13; H, 5.55; N, 12.30.

*4.1.7.28. N-(3-Methylpyridin-2-yl)-2-(4-((8-(trifluoromethyl)quinolin-4-yl)amino)phenyl)propanamide (**TPA28**).* Obtained following

the general procedure by the condensation between acid **47** and 2-amino-3-methylpyridine. Yield 78%. Mp 230–232 °C. ^{1}H NMR (DMSO-d_6) δ 1.40 (d, J = 6.5 Hz, 3H), 2.02 (s, 3H), 3.97 (q, J = 6.5 Hz, 1H), 6.95 (m, 1H), 7.18 (m, 1H), 7.34 (m, 4H), 7.46 (m, 1H), 7.62 (m, 2H), 8.10 (m, 1H), 8.53 (m, 1H), 8.70 (m, 1H), 9.20 (s, 1H), 10.16 (s, 1H), 12.31 (s, 1H). ^{13}C NMR (DMSO-d_6) δ 25.3, 26.1, 52.2, 110.0, 115.1, 119.1, 124.0, 124.3, 128.9, 129.1, 129.6, 136.1, 136.2, 144.4, 153.5, 155.1, 155.8, 157.9, 183.2. IR (Nujol) 1663, 1583 cm^{-1}. Anal. Calcd. for $C_{25}H_{21}F_3N_4O$ (450.45): C, 66.66; H, 4.70; N, 12.44. Found: C, 66.60; H, 4.71; N, 12.47.

*4.1.7.29. N-(3-Methylpyridin-2-yl)-2-(4-((7-(trifluoromethyl)quinolin-4-yl)amino)phenyl)propanamide (**TPA29**).* Obtained following the general procedure by the condensation between acid **48** and 2-amino-3-methylpyridine. Yield 83%. Mp 112–114 °C. ^{1}H NMR (DMSO-d_6) δ 1.45 (d, J = 6.5 Hz, 3H), 2.01 (s, 3H), 3.96 (q, J = 6.5 Hz, 1H), 6.98 (m, 1H),7.35 (m, 4H), 7.47 (m, 1H), 7.80 (m, 2H), 8.56 (m, 1H), 8.63 (m, 2H) 9.19 (m, 1H), 10.17 (s, 1H). ^{13}C NMR (DMSO-d_6) δ 25.3, 26.1, 52.2, 110.0, 116.8, 121.9, 122.8, 123.1, 124.3, 129.1, 130.2, 133.5, 136.1, 136.2, 144.4, 150.2, 153.5, 154.3, 155.8, 183.2. IR (Nujol) 1671, 1587 cm^{-1}. Anal. Calcd. for $C_{25}H_{21}F_3N_4O$ (450.45): C, 66.66; H, 4.70; N, 12.44. Found: C, 66.71; H, 4.72; N, 12.40.

*4.1.8. Ethyl 2-(2-(4-((2-(trifluoromethyl)pyridin-4-yl)amino) phenyl)propanamido)acetate (**8**)*

The acid **7** (0.62 g, 2 mmol), EDC (0.39 g, 2.2 mmol) and HOBt (0.27 g, 2 mmol) were dissolved in MeCN (10 mL). The mixture was stirred at r.t. for 30 min, then TEA (0.4 mL, 4 mmol) and ethyl glicinate hydrochloride (0.56 g, 4 mmol) were added. The mixture was stirred at r.t. for 4 h. After the solvent was removed under vacuum. The residue was dissolved in AcOEt (20 mL) and washed sequentially with brine (2 × 5 mL), 10% citric acid (2 × 5 mL), saturated $NaHCO_3$ aqueous solution (2 × 5 mL) and water (2 × 5 mL). The organic layer was dried over anhydrous Na_2SO_4 and evaporated under vacuum. The residue was treated with iPr_2O; the precipitate was then filtrated and purified by recrystallization from 2-propanol (2-PrOH). Yield 80%. Mp 90–91 °C. ^{1}H NMR (DMSO-d_6) δ 1.27 (t, J = 7.2 Hz, 3H), 1.39 (d, J = 6.8 Hz, 3H), 3.79 (m, 3H), 4.15 (q, J = 7.2 Hz, 2H), 7.07 (m, 1H), 7.20 (m, 3H), 7.36 (m, 2H), 8.30 (m, 2H), 10.02 (s, 1H),. IR (Nujol) 1724, 1636, 1605, 1592 cm^{-1}. Anal. Calcd. for $C_{19}H_{20}F_3N_3O_3$ (395.38): C, 57.72; H, 5.10; N, 10.63. Found: C, 57.77; H, 5.11; N, 10.60.

*4.1.9. (2-(4-((2-(Trifluoromethyl)pyridin-4-yl)amino)phenyl) propanoyl)glycine (**9**)*

The ester **8** (0.40 g, 1 mmol) was dissolved in EtOH (10 mL). To this solution a 5 N aqueous NaOH (2 mL) and water (2 mL) were added. The resulting mixture was stirred at r.t. for 24 h. After removing EtOH under vacuum, ice and then aqueous 20% HCl solution until pH 3-4 were added. The formed precipitate was filtrated, washed with water and re-crystallized with EtOH. Yield 94%. Mp 229–231 °C. ^{1}H NMR (DMSO-d_6) δ 1.33 (d, J = 7.5, 3H), 3.72 (m, 3H), 7.04 (m, 1H), 7.17 (m, 3H), 7.34 (m, 2H), 8.28 (m, 2H), 9.19 (s, 1H), 12.46 (s, 1H). IR (Nujol) 3350, 3281, 2854, 2522, 1900, 1707, 1657, 1606 cm^{-1}. Anal. Calcd. for $C_{17}H_{16}F_3N_3O_3$ (367.32): C, 55.59; H, 4.39; N, 11.44. Found: C, 55.54; H, 4.38; N, 11.47.

*4.1.10. Methyl (E)-2-(4-((5,5,5-trifluoro-4-oxopent-2-en-2-yl) amino)phenyl)acetate (**11**)*

Was prepared using the same procedure used for the synthesis of the compound **4**, starting from methyl 2-(4-aminophenyl)acetate **10**. Yield 96%. Mp 164–165 °C. ^{1}H NMR (DMSO-d_6) δ 2.24 (s, 3H), 3.54 (s, 2H), 3.98 (s, 3H), 5.82 (s, 1H), 7.34 (d, J = 7.6 Hz, 2H), 7.81 (d, J = 7.6 Hz, 2H), 12.52 (s, 1H). IR (Nujol) 3260, 1717 cm^{-1}. Anal. Calcd. for $C_{14}H_{14}F_3NO_3$ (301.26): C, 55.82; H, 4.68; N, 4.65. Found: C, 55.87; H, 4.67; N, 4.67.

*4.1.11. Methyl 2-(4-(((1E,3E)-1-(dimethylamino)-6,6,6-trifluoro-5-oxohexa-1,3-dien-3-yl)amino)phenyl)acetate (**12**)*

Prepared using the same procedure used for the synthesis of the compound **5**, starting from ester **11**. Yield 95%. Mp 105–106 °C (*n*-hexane). ^{1}H NMR (DMSO-d_6) δ 2.77 (s, 3H), 3.28 (s, 3H), 3.92 (s, 3H), 4.03 (s, 2H), 5.02 (d, J = 12.8 Hz, 1H), 5.96 (s, 1H), 7.49 (m, 2H), 8.03 (m, 3H), 12.86 (s, 1H). IR (Nujol) 1724, 1661 cm^{-1}. Anal. Calcd. for $C_{17}H_{19}F_3N_2O_3$ (356.34): C, 57.30; H, 5.37; N, 7.86. Found: C, 57.34; H, 5.36; N, 7.82.

*4.1.12. Methyl 2-(4-((2-(trifluoromethyl)pyridin-4-yl)amino) phenyl)acetate (**13**)*

Prepared using the same procedure used for the synthesis of compound **6**, starting from ester **12**. Yield 90%. Mp 48–50 °C (*n*-hexane).^{1}H NMR (DMSO-d_6) δ 3.58 (s, 2H), 3.93 (s, 3H), 6.93 (m, 1H), 7.18 (m, 2H), 7.59 (m, 2H), 7.72 (m, 1H), 8.48 (m, 1H), 9.70 (s, 1H). IR (Nujol) 3362, 3205, 1717 cm^{-1}. Anal. Calcd. for $C_{15}H_{13}F_3N_2O_2$ (310.27): C, 58.07; H, 4.22; N, 9.03. Found: C, 58.03; H, 4.23; N, 9.06.

*4.1.13. 2-(4-((2-(Trifluoromethyl)pyridin-4-yl)amino)phenyl)acetic acid (**14**)*

Prepared using the same procedure used for the synthesis of **7**, starting from ester **13**. Yield 84%. Mp 219–220 °C· ^{1}H NMR (DMSO-d_6) δ 3.67 (s, 2H), 7.19 (m, 1H), 7.31 (m, 3H), 7.40 (d, J = 8.4 Hz, 2H), 8.40 (d, J = 5.8 Hz, 1H), 9.33 (s, 1H). IR (Nujol) 3325, 2495, 1898, 1693 cm^{-1}. Anal. Calcd. for $C_{14}H_{11}F_3N_2O_2$ (296.24): C, 56.76; H, 3.74; N, 9.46. Found: C, 56.71; H, 3.73; N, 9.48.

*4.1.14. Methyl 2-methyl-2-(4-nitrophenyl)propanoate (**16**)*

Methyl ester **15** (1.56 g, 8 mmol) was dissolved in anhydrous DMF (20 mL). The solution was cooled to 0 °C, then NaH (0.63 g, 16 mmol, 60% dispersion in oil) was added slowly and cautiously. The resulting mixture was allowed to warm to r.t. and then stirred for additional 20 min. The solution was cooled again to 0 °C. Iodomethane (2 mL, 32 mmol) was added dropwise, and the resulting solution was allowed to stir at 0 °C. for about 30 min. The solution was warmed to r.t. and stirred for additional 1 h. The solution was cooled to 0 °C and quenched with water, maintaining 0 °C throughout the quenching process. The obtained mixture was extracted with dichloromethane (CH_2Cl_2) (2 × 15 mL). The combined organic layers were washed with water (2 × 5 mL) and brine (2 × 5 mL); dried over anhydrous Na_2SO_4. After removing the Na_2SO_4 by filtration, the filtrate was concentrated under vacuum. The residue was purified by column chromatography (silica gel, 8:1 petroleum ether: AcOEt) and gave the title compound as a yellow solid material. Yield 80%. Mp. 33–35 °C. lit. 45–46 °C [26]. ^{1}H NMR (DMSO-d_6) δ 1.69 (s, 6H), 3.74 (s, 3H), 7.45 (d, J = 8.5 Hz, 2H), 8.13 (d, J = 8.5 Hz, 2H). Anal. Calcd. for $C_{11}H_{13}NO_4$ (223.22): C, 59.19; H, 5.87; N, 6.27. Found: C, 59.24; H, 5.86; N, 6.30.

*4.1.15. Methyl 2-(4-aminophenyl)-2-methylpropanoate (**17**)*

To a solution of ester **16** (1.34 g, 6 mmol) in EtOH (15 mL) tin (II) chloride dihydrate (5.5 g, 24 mmol) was added. The resulting solution was stirred at 85 °C for 4 h. After cooling, the pH was adjusted to 10 with 40% aqueous NaOH. The mixture was extracted with AcOEt (3 × 5 mL). The combined organic layers were washed with water (2 x 5 mL) and brine (2 × 5 mL) and dried over Na_2SO_4. After removing of the Na_2SO_4 the filtrate was concentrated under vacuum to obtain the title compound as yellow oil. Yield 87%. ^{1}H NMR (DMSO-d_6) δ 0.63 (s, 3H), 0.91 (s, 3H), 3.54 (s, 3H), 4.96 (s, 2H), 6.49 (d, J = 8.5 Hz, 2H), 6.91 (d, J = 8.5 Hz, 2H). IR (Film) 3435, 3349, 2956, 1723, 1626 cm^{-1}. Anal. Calcd. for $C_{11}H_{15}NO_2$ (193.24): C, 68.37; H, 7.82; N, 7.25. Found: C, 68.31; H, 7.85; N, 7.23.

*4.1.16. Methyl (E)-2-methyl-2-(4-((5,5,5-trifluoro-4-oxopent-2-en-2-yl)amino)phenyl)propanoate (**18**)*

Prepared using the same procedure used for the synthesis of the compound **4**, starting from ester **17**. Yield 87%.Oil. ^{1}H NMR (DMSO-d_6) δ 1.53 (s, 6H), 2.27 (s, 3H), 3.77 (s, 3H), 5.77 (s, 1H), 7.01 (d, J = 8.5 Hz, 2H), 7.77 (d, J = 8.5 Hz, 2H), 12.58 (s, 1H). IR (Film) 2925, 1721, 1571 cm^{-1}. Anal. Calcd. for $C_{16}H_{18}F_3NO_3$ (329.31): C, 58.35; H, 5.51; N, 4.25. Found: C, 58.30; H, 5.52; N, 4.27.

*4.1.17. 2-Methyl-2-(4-((2-(trifluoromethyl)pyridin-4-yl)amino) phenyl)propanoic acid (**21**)*

A mixture of **18** (1.65 g, 5 mmol) and DMF-DMA (1.79 g, 15 mmol) in anhydrous toluene (20 mL) was refluxed for 1 h, then allowed to reach the room temperature and stirred for additional 24 h. The mixture was carefully concentrated in vacuum. Without isolate the dienaminone intermediate (**19**) the residue was dissolved in dry DMF (5 mL), ammonium acetate (0.31 g, 4 mmol) was added and the mixture was gently heated for 1.5 h. The mixture was carefully concentrated in vacuum, and then ice-water (15 mL) was added. The formed solid was filtered off and washed with water. The obtained trifluoromethylpyridine ester (**20**) was dissolved in EtOH (20 mL), 5 N solution of NaOH (4 mL) and water (4 mL) were added. The resulting mixture was stirred at r.t. for 24 h. After removing EtOH under vacuum, the residue was ice added and the resulting mixture acidified with aqueous 20% HCl solution until pH 3-4. The formed precipitate was filtered and washed with water. Yield 42%. Mp 173–175 °C. ^{1}H NMR (DMSO-d_6) δ 1.48 (s, 6H), 7.02 (m, 1H), 7.17 (m, 3H), 7.52 (m, 2H), 8.28 (m, 1H), 9.25 (s, 1H). IR (Nujol) 3285, 2924, 1690, 1623, 1602 cm^{-1}. Anal. Calcd. for $C_{16}H_{15}F_3N_2O_2$ (324.30): C, 59.26; H, 4.66; N, 8.64. Found: C, 59.19; H, 4.64; N, 8.67.

*4.1.18. General procedure for the synthesis of esters **22-25***

Compound **15** (2.50 g, 12.8 mmol) was dissolved in anhydrous DMF (20 mL). The solution was cooled to 0 °C. NaH (1.02 g, 25.6 mmol, 60% dispersion in oil) was added slowly and cautiously. The resulting mixture was allowed to warm to r.t. and was stirred for additional 20 min. The solution was cooled again to 0 °C The appropriate dihaloalkane (25.6 mmol) was added dropwise, and the resulting solution was allowed to stir at 0 °C for 30 min. The solution was warmed to r.t. and stirred for additional 1 h. The solution was cooled to 0 °C and quenched with water, maintaining 0 °C throughout the quenching process. The obtained mixture was extracted with CH_2Cl_2 (2 × 20 mL). The combined organic layers were washed with water and brine and dried over Na_2SO_4. This was removed by filtration and the filtrate concentrated under vacuum to give the crude esters **22-25** (see supplementary data for physical and spectral data).

*4.1.19. General procedure for the synthesis of esters **26-29***

To a solution of ester **22-25** (9.78 mmol) in AcOEt (230 mL) stannous chloride hydrate (110 g, 48.9 mmol was added). The reaction mixture was stirred at 75 °C for 4 h. Reaction mixture was cooled at r.t and then diluted with AcOEt (100 mL) and 25% aqueous ammonia solution until pH 10 was added. The organic layer was separated out, dried over Na_2SO_4 and the solvent evaporated under vacuum to obtain the desired compound **26-29** (see supplementary data for physical and spectral data).

*4.1.20. General procedure for the synthesis of acids **42–45***

To a solution of dienaminone **34-37** (2 mmol) in dry DMF (5 mL), ammonium acetate (0.308 g, 4 mmol) was added and the mixture was gently refluxed for 1.5 h. The mixture was carefully concentrated in vacuum, and then ice-water (15 mL) was added. The formed solid was dissolved in EtOH (20 mL), this solution was added with 5 N solution of NaOH (4 mL) and water (4 mL). The resulting mixture was stirred at r.t. for 20 h. After removing EtOH under vacuum ice was added and then aqueous 20% HCl solution until pH 3-4. The formed precipitate was filtered and washed with water and dried.

*4.1.20.1. 1-(4-((2-(Trifluoromethyl)pyridin-4-yl)amino)phenyl)cyclopropane-1-carboxylic acid (**42**).* Prepared using the general procedure starting from dienaminone **34**. Yield 59%. Mp 208–210 °C. ^{1}H NMR (DMSO-d_6) δ 1.13 (m, 2H), 1.45 (m, 2H), 7.10 (m, 1H), 7.16 (m, 2H), 7.23 (m, 1H), 7.33 (m, 2H), 8.29 (s, 1H), 9.34 (s, 1H). IR (Nujol) 3285, 2924, 1677, 1602 cm^{-1}. Anal. Calcd. for $C_{16}H_{13}F_3N_2O_2$ (322.28): C, 59.63; H, 4.07; N, 8.69. Found: C, 59.68; H, 4.06; N, 8.71.

*4.1.20.2. 1-(4-((2-(Trifluoromethyl)pyridin-4-yl)amino)phenyl)cyclobutane-1-carboxylic acid (**43**).* Prepared using the general procedure starting from dienaminone **35**. Yield 78%. Mp 184–186 °C. ^{1}H NMR (DMSO-d_6) δ 1.75 (m, 1H), 1.96 (m, 1H), 2.38 (m, 2H), 2.70 (m, 2H), 7.08 (m, 1H), 7.21 (m, 3H), 7.30 (m, 2H), 8.28 (s, 1H), 9.26 (s, 1H). IR (Nujol) 3319, 2855, 1671, 1622, 1606 cm^{-1}. Anal. Calcd. for $C_{17}H_{15}F_3N_2O_2$ (336.31): C, 60.71; H, 4.50; N, 8.33. Found: C, 60.77; H, 4.48; N, 8.37.

*4.1.20.3. 1-(4-((2-(Trifluoromethyl)pyridin-4-yl)amino)phenyl)cyclopentane-1-carboxylic acid (**44**).* Prepared using the general procedure starting from dienaminone **36**. Yield 86%.Mp > 250 °C. ^{1}H NMR (DMSO-d_6) δ 1.65 (m, 4H), 1.79 (m, 4H), 7.07 (m, 1H), 7.18 (m, 3H), 7.34 (m, 2H), 8.27 (s, 1H), 9.27 (s, 1H), 12.24 (s, 1H). IR (Nujol) 3301, 2921, 1691, 1618, 1601 cm^{-1}. Anal. Calcd. for $C_{18}H_{17}F_3N_2O_2$ (350.33): C, 61.71; H, 4.89; N, 8.00. Found: C, 61.65; H, 4.88; N, 8.04.

*4.1.20.4. 1-(4-((2-(Trifluoromethyl)pyridin-4-yl)amino)phenyl)cyclohexane-1-carboxylic acid (**45**).* Prepared using the general procedure starting from dienaminone **37**. Yield 88%. Mp > 250 °C. ^{1}H NMR (DMSO-d_6) δ 1.22 (m, 1H), 1.43 (m, 1H), 1.59 (m, 6H), 2.64 (m, 2H), 7.07 (m, 1H), 7.18 (m, 3H), 7.39 (m, 2H), 8.27 (s, 1H), 9.28 (s, 1H). IR (Nujol) 3305, 1687, 1622, 1603, 1523, 1459, 1364, 1320, 1229, 1178 cm^{-1}. Anal. Calcd. for $C_{19}H_{19}F_3N_2O_2$ (364.36): C, 62.63; H, 5.26; N, 7.69. Found: C, 62.60; H, 5.30; N, 7.72.

*4.1.20.5. 2-(4-Aminophenyl)propanoic acid (**46**).* To a solution of the ester **2** (1.79 g, 10 mmol) in EtOH (50 mL) 5 N solution of NaOH (20 mL) and water (20 mL) were added. The resulting mixture was stirred at r.t. for 24 h. After removing EtOH under vacuum to the resulting solution ice was added and then 20% aqueous HCl solution until pH 3-4. The formed precipitate was filtered, washed with water, dried and re-crystallized from EtOH. Yield 97%. Mp 123–125 °C. ^{1}H NMR (DMSO-d_6) δ 1.26 (d, J = 7.0 Hz, 3H), 3.43 (q, J = 7.0 Hz, 1H), 6.48 (d, J = 8.5 Hz, 2H), 6.90 (d, J = 8.5 Hz, 2H). IR (Nujol) 2854, 2610, 2188, 1632, 1591 cm^{-1}. Anal. Calcd. for $C_9H_{11}NO_2$ (165.19): C, 65.44; H, 6.71; N, 8.48. Found: C, 65.48; H, 6.68; N, 8.52.

*4.1.21. General procedure for the synthesis of acids **47-48***

A solution of acid **46** (0.34 g, 2 mmol) in EtOH (40 mL) was added with the appropriate 4-chloroquinoline (2 mmol) and refluxed for 24 h. Then the solvent was removed under vacuum and the formed solid was filtered, treated with iPr_2O, filtered and then dried.

*4.1.21.1. 2-(4-((8-(Trifluoromethyl)quinolin-4-yl)amino)phenyl)propanoic acid (**47**).* Obtained starting from 4-chloro-8-trifluoromethylquinoline. Yield 89%. Mp 158–160 °C. ^{1}H NMR (DMSO-d_6) δ 1.42 (m, 3H), 4.09 (m, 1H), 6.93 (m, 1H), 7.45 (m, 4H), 7.87 (m, 1H), 8.38 (m, 1H), 8.46 (m, 1H), 9.08 (m, 1H). IR (Nujol) 2926, 1726, 1619, 1589 cm^{-1}. Anal. Calcd. for $C_{19}H_{15}F_3N_2O_2$ (360.33):

C, 63.33; H, 4.20; N, 7.77. Found: C, 63.38; H, 4.19; N, 7.80.

*4.1.21.2. 2-(4-((7-(Trifluoromethyl)quinolin-4-yl)amino)phenyl) propanoic acid (**48**).* Obtained starting from 4-chloro-7-trifluoromethylquinoline. Yield 87%. Mp 163–165 °C. ^{1}H NMR (DMSO-d_6) δ 1.41 (m, 3H), 3.80 (m, 1H), 6.90 (m, 1H), 7.44 (m, 2H), 7.49 (m, 2H), 8.12 (m, 1H), 8.45 (m, 1H), 8.60 (m, 1H), 9.03 (m, 1H), 11.16, (s, 1H), 12.40 (s, 1H, OH). IR (Nujol) 2960, 1720, 1598 cm^{-1}. Anal. Calcd. for $C_{19}H_{15}F_3N_2O_2$ (360.33): C, 63.33; H, 4.20; N, 7.77. Found: C, 63.30; H, 4.23; N, 7.74.

4.2. Biological assays

4.2.1. Preparation of rat, mouse brain and HeLa transfected cells homogenates

Brains (minus cerebella) from adult Wistar or Sprague-Dawley rats (killed by decapitation) and from male B6CBAF1/J mice (killed by cervical dislocation), stored at −80 °C, were thawed, weighed and homogenized in cold buffer (20 mM HEPES, 1 mM $MgCl_2$ pH 7.0). Homogenates were centrifuged (35,000 g at 4 °C for 20 min) before the pellet was resuspended in cold homogenization buffer. Centrifugation and resuspension was repeated twice. The suspension was incubated at 37 °C for 15 min to degrade any endogenous substrate able to interfere with the FAAH assay. After centrifugation (35,000 g at 4 °C for 20 min), the pellet was resuspended in cold buffer (50 mM Tris-HCl, 1 mM EDTA, 3 mM $MgCl_2$, pH 7.4). The protein concentration was determined according to reported method [27] after which the samples were frozen in aliquots at −80 °C. The homogenates from HeLa cells transfected with FAAH wt and FAAH T488A were performed as previously reported [12].

4.2.2. Assay of [^{3}H]AEA hydrolysis in the homogenates

The assays were performed with minor modifications of our previously described method [28]. Briefly, homogenates in assay buffer (10 mM Tris-HCl, 1 mM EDTA, pH 7.4) were mixed with test **TPA** dissolved in ethanol or DMSO on ice. Hydrolysis reactions were initiated by addition of substrate ([^{3}H]AEA in 10 mM Tris-HCl, 1 mM EDTA, pH 7.4 containing 10 mg/mL fatty acid-free bovine serum, assay concentration 0.5 μM unless otherwise stated) and incubation at 37 °C. For the brain homogenates, hydrolysis at 37 °C was allowed to proceed for 10 min (assay volume was 200 μL, with 1 and 0.3 μg/assay protein concentrations of the rat and mouse homogenates, respectively). For the transfected cells, a 2 h incubation was used. For the kinetic experiments, the AEA: fatty acid-free bovine serum albumin ratio was kept constant at 1: ~4.5 (μM). Following incubation, reactions were stopped by addition of 400 μL activated charcoal (80 μL activated charcoal + 320 μL 0.5 M HCl) and placement of samples on ice before centrifugation at 2500 rpm for 10 min. Aliquots (200 μL) of the supernatant were analyzed for tritium content by liquid scintillation spectroscopy with quench correction. Sample sizes were chosen on the basis of previous data investigating FAAH inhibitory properties of compounds. IC_{50} values were calculated by fitting the data (as % of control) to the algorithm log (inhibitor) vs. response − Variable slope (four parameters) built into the GraphPad prism programme (versions 5-7 for the Macintosh; GraphPad Software Inc., San Diego, CA, USA). The equation used is Y=Bottom + (Top-Bottom)/(1 + 10^((LogIC50-X)*HillSlope)). Two constraints were used: one where the top (uninhibited) value was set to 100 and the bottom (maximum inhibition) value was set to 0 and one where only the top value was constrained. The curve fits were then compared using Akaike's Informative Criteria. When the best fit had a bottom value > 0, this is shown in the results as "maximum inhibition", where the value given is 100- the calculated bottom value. For the kinetic experiments, the data was analysed using algorithms for competitive, mixed-type or non-competitive inhibition in the GraphPad Prism programme, and the best fit determined using Akaike's Informative Criteria. Using the methodology reported here, carprofen has been shown to inhibit rat brain AEA (0.5 μM) hydrolysis with an IC_{50} value of 32 μM [24]. Arachidonoylserotonin inhibited 2 μM AEA hydrolysis with an IC_{50} value of 1.2 μM [29]. URB597 is an irreversible inhibitor, and thus its potency will be dependent upon the preincubation time used. In our hands, the compound inhibits 2 μM AEA hydrolysis following a 10 min preincubation period with IC_{50} values of 64 and 18 nM at assay pH values of 6 and 8, respectively [30].These values are consistent with the literature using other assays [31–33].

4.2.3. COX assays

The assay of Meade et al. [34] with minor modifications [35] was used. Briefly, buffer containing 1 μM haematin, 2 mM phenol, 5 mM EDTA, substrate (arachidonic acid or 2-AG, 10 μM final concentration) and 0.1 M Tris–HCl, pH 7.4 at room temperature was added to an oxygen electrode chamber with an integral stirring unit (Oxygraph System, Hansatech Instruments, King'sLynn, U.K.). The final assay volume was 2 mL, and the oxygen electrode was calibrated with respect to air pressure and r.t. After addition of 20 mL test compound dissolved in EtOH, a baseline was established over a period of 5 min. Reactions were started by addition of COX (ovine COX-1 or human recombinant COX-2, as appropriate, 200U per assay), and the oxygen consumption was measured in 10 s blocks. Data are presented as the change in oxygen consumption (μM) from the point of addition of the enzyme.

4.3. Molecular docking

Rigid docking calculations were performed using the software Autodock 4.2 [36]. The 3D structures of compounds were built with Pymol 1.74. Docking was performed on a single monomer of rat FAAH (PDB code 3QK5) [37], after crystallized ligand and water removal. Lys^{142} was considered in the basic form according to the proposed catalytic mechanism [38]. Rigid docking in the competitive binding site was performed using a cubic docking box of 60^3 grid points, centered on the monomer A of rat FAAH active site. The rotatable bonds of the compound were automatically detected by Autodock default settings. For each docking run, 100 iterations were performed using default parameters of Lamarckian genetic algorithm (GALS). The results were clustered on the basis of RMSD criterion (≤4 Å). The energetically favored poses of the best clusters, according to Autodock 4.2 score, were loaded in the two monomers of the dimeric form of rat FAAH and each system were used for further analysis.

4.4. Molecular dynamics

MD simulations were performed to refine best docking results with Amber15 [39]. Each complex was immersed in a pre-equilibrated octahedral box of TIP3P water molecules, and the system was neutralized. The final system contained about 80000 atoms. All simulations were performed with the Amber 99SBildn force field [40] for the protein and the gaff force field [39] for the ligands. The charge distribution of the inhibitors was refined using RESP charges [41] fitted to the B3LYP/6-31G(d) electrostatic potential obtained with Gaussian09 [42]. For each complex the geometry was minimized using convergence criterion for the energy gradient set to 0.01 kcal/mol·Å^2 in three steps, which involve: i) hydrogen atoms in the system (5000 steps of steepest descent and 10000 steps of conjugate gradient), ii) hydrogen atoms, water molecules and counterions (2000 steps of steepest descent and 18000 steps of conjugate gradient), iii) finally the whole system

(2000 steps of steepest descent and 18000 steps of conjugate gradient). Thermalization of the system was performed in four steps of 60 ps, increasing the temperature from 50 to 298 K. Concomitantly, the atoms that define the protein backbone were restrained during thermalization using a variable restraining force. Thus, a force constant of 30 kcal/mol·Å^2 was used in the first stage of the thermalization and was subsequently decreased by increments of 5 kcal/mol·Å^2 in the next stages. Then, an additional step of 250 ps was performed in order to equilibrate the system density at constant pressure (1 bar) and temperature (298 K). Finally, an extended trajectory was run using a time step of 2 fs. SHAKE was used for those bonds containing hydrogen atoms in conjunction with periodic boundary conditions at constant pressure and temperature, particle mesh Ewald for the treatment of long range electrostatic interactions, and a cutoff of 9 Å for non-bonded interactions. The structural analysis was performed using in-house software and standard codes of AmberTools 15.

4.5. Free energy calculations

Analysis of the MD trajectory was carried out by calculating Molecular Mechanics Generalized Born Surface Area (MM/GBSA) [15], and Solvated Interaction Energy (SIE) [16], on a 0.1 ns interval at the end of the trajectories. We used open source AmberTools package (MMPBSA.py) [43] to perform binding free energy calculations.

4.6. QM/MM calculations

The contribution due to the formation of the ligand-protein complex in the gas phase was determined by QM/MM calculations. To this end, the ligand was treated at the QM level and all the residues within 15 Å of the ligand were treated classically. Accordingly, the electrostatic term accounts for the QM interaction (determined at the B3LYP/6-311 + G(d,p) level) of the ligand with the set of point charges of the residues included in the MM region. QM/MM calculations were performed with Gaussian09 [42] for a set of 50 snapshots taken on a 0.1 ns interval along the last 5 ns of the trajectories, averaging the electrostatic and van der Waals components of the individual snapshots. The van der Waals term was determined using the 6-12 expression as implemented in AMBER. The contribution due to the solvation of the complexes (ΔG_{sol}) was calculated by MM/GBSA and MM/PBSA methods.

4.7. Thermodynamic integration

The A1-mode binding of **TPA1** in monomer A of rFAAH was used as starting structure for the free energy calculation using TI. The TI simulations of the alchemical transformation from **TPA1** into **TPA4**,**TPA11**, **TPA13** or **TPA14** using a single step soft-core potentials approach [44], implemented in Amber15 [39]. Relative free energies were calculated using 9 different coupling parameters (λ), where $\lambda = 0$ is the initial state and $\lambda = 1$ is the final state [45]. Each window was subjected to a 1000-step steepest descent minimization to remove bad initial contacts and a 50 ps NPT heating run in which the system temperature was raised to 298 K with a target pressure of 1 bar. Equilibration was followed by a 5 ns NPT simulation for data collection. Altogether, TI simulation required at least 90 ns MD simulation, since it includes 2 transformations of 9 windows.

The following equation was used to derive the MD simulation settings for each window.

$$\Delta G = \int_0^1 \frac{\partial V(\lambda)}{\delta \lambda}\, \delta\lambda$$

4.8. Homology building

The amino acid sequence of mouse FAAH was retrieved from the Universal Protein Resource database (http://www.uniprot.org accession ID O08914). The 3D structure of the target protein was modeled using SWISSMODEL [46]. The X-ray determined structure of rat FAAH 3QKV was used as template (covered sequence 100%; sequence identity of 91.6%). The global model quality estimation yielded a score of 0.92.

Authors will release the atomic coordinates upon publication.

Acknowledgments

This work was supported by grants from the Regione Autonoma della Sardegna (Project L.R. 7/2007, no. 2012_CRP-59473) to VO; the Swedish Research Council (Grant no. 12158, medicine) and the Research Funds of the Medical Faculty, Umeå University to CJF; the Generalitat de Catalunya (2014SGR1189), ICREA Academia, and Consorci de Serveis Universitaris de Catalunya to FJL. CMM and BC acknowledge the CINECA (ISCRA C projects ID HP10C34LJ7, HP10CPFIRC and HP10CSJ2H8) for the access to high performance computing resources.

Appendix B. Supplementary data

Supplementary data related to this article can be found at http://dx.doi.org/10.1016/j.ejmech.2017.05.033.

These data include additional figures and tables illustrating: i) computational data, ii) alignment and superimposition of mouse and rat FAAH, iii) general synthetic procedure, physical and spectral data for compounds **22-37**, and **42-45**, iv) FAAH inhibitory activity in HeLa cell homogenates expressing wild type and mutant FAAH v) Molecular Formula Strings Spreadsheet.

References

[1] C.J. Fowler, The potential of inhibitors of endocannabinoid metabolism as anxiolytic and antidepressive drugs - a practical view, Eur. Neuropsychopharmacol. 25 (2015) 749–762.
[2] J.R. Clapper, R.A. Mangieri, D. Piomelli, The endocannabinoid system as a target for the treatment of cannabis dependence, Neuropharmacology 56 (suppl 1) (2009) 235–243.
[3] K.M. Jung, G. Astarita, S. Yasar, V. Vasilevko, D.H. Cribbs, E. Head, C.W. Cotman, D. Piomelli, An amyloid β(42)-dependent deficit in anandamide mobilization is associated with cognitive dysfunction in Alzheimer's disease, Neurobiol. Aging 33 (2012) 1522–1532.
[4] L. Carnevali, S. Rivara, E. Nalivaiko, J.F. Thayer, F. Vacondio, M. Mor, A. Sgoifo, Pharmacological inhibition of FAAH activity in rodents: a promising pharmacological approach for psychological-cardiac comorbidity? Neurosci, Biobehav. Rev. 74 (Pt B) (2017) 444–452.
[5] W. Tuo, N. Leleu-Chavain, J. Spencer, S. Sansook, R. Millet, P. Chavatte, Therapeutic potential of fatty acid amide hydrolase, monoacylglycerol lipase, and N-Acylethanolamine acid amidase inhibitors J, Med. Chem. 60 (2017) 4–46.
[6] J.P. Huggins, T.S. Smart, S. Langman, L. Taylor, T. Young, An efficient randomised, placebo-controlled clinical trial with the irreversible fatty acid amide hydrolase-1 inhibitor PF-04457845, which modulates endocannabinoids but fails to induce effective analgesia in patients with pain due to osteoarthritis of the knee, Pain 153 (2012) 1837–1846.
[7] Sanofi, Clinical Studies of the FAAH Inhibitor SSR411298, 2016. http://en.sanofi.com/img/content/study/DFI10560_summary.pdf.
[8] C. Mallet, C. Dubray, C. Dualé, FAAH inhibitors in the limelight, but regrettably, Int. J. Clin. Pharmacol. Ther. 54 (7) (2016) 498–501.
[9] Cyclica Predicts Mechanism of Neurotoxicity for BIA 10-2474, an Experimental Drug Causing Death in Clinical Trial, 2016. https://cyclicarx.com/bia-10-2474/.

[10] S. Holt, B. Paylor, L. Boldrup, K. Alajakku, S. Vandevoorde, A. Sundström, M.T. Cocco, V. Onnis, C.J. Fowler, Inhibition of fatty acid amide hydrolase, a key endocannabinoid metabolizing enzyme, by analogues of ibuprofen and indomethacin, Eur. J. Pharmacol. 56 5 (1–3) (2007) 26–36.
[11] C.J. Fowler, E. Björklund, A.H. Lichtman, P.S. Naidu, C. Congiu, V. Onnis, Inhibitory properties of ibuprofen and its amide analogues towards the hydrolysis and cyclooxygenation of the endocannabinoid anandamide, J. Enzyme Inhib. Med. Chem. 28 (1) (2013) 172–182.
[12] J. Karlsson, C.M. Morgillo, A. Deplano, G. Smaldone, E. Pedone, F.J. Luque, M. Svensson, E. Novellino, C. Congiu, V. Onnis, B. Catalanotti, C.J. Fowler, Interaction of the N-(3-Methylpyridin-2-yl)amide derivatives of flurbiprofen and ibuprofen with FAAH: enantiomeric selectivity and binding mode, PLoS One 10 (11) (2015) e0142711.
[13] M.T. Cocco, C. Congiu, V. Lilliu, V. Onnis, Synthesis of new N-(2-(trifluoromethyl)pyridin-4-yl)anthranilic acid derivatives and their evaluation as anticancer agents, Bioorg. Med. Chem. Lett. 14 (2004) 5787–5791.
[14] C.W. Alexander, D. De, I.K. Khanna, S. Pillarisetti, Preparation of Novel Heterocyclic Compounds as GATA Modulators, Patent WO2010028179A1, 2010.
[15] T. Hou, J. Wang, Y. Li, W. Wang, Assessing the performance of the MM/PBSA and MM/GBSA methods. 1. The accuracy of binding free energy calculations based on molecular dynamics simulations, J. Chem. Inf. Model 51 (2011) 69–82.
[16] M. Naïm, S. Bhat, K.N. Rankin, S. Dennis, S.F. Chowdhury, I. Siddiqi, P. Drabik, T. Sulea, C.I. Bayly, A. Jakalian, E.O. Purisima, Solvated interaction energy (SIE) for scoring protein-ligand binding affinities. 1. Exploring the parameter space, J. Chem. Inf. Model 47 (2007) 122–133.
[17] M. Mileni, J. Garfunkle, J.K. DeMartino, B.F. Cravatt, D.L. Boger, R.C. Stevens, Binding and inactivation mechanism of a humanized fatty acid amide hydrolase by alpha-ketoheterocycle inhibitors revealed from cocrystal structures, J. Am. Chem. Soc. 131 (2009) 10497–10506.
[18] M. Mileni, J. Garfunkle, C. Ezzili, F.S. Kimball, B.F. Cravatt, R.C. Stevens, D.L. Boger, X-ray crystallographic analysis of alpha-ketoheterocycle inhibitors bound to a humanized variant of fatty acid amide hydrolase, J. Med. Chem. 53 (2010) 230–240.
[19] R.C. Stevens, A.H. Lichtman, B.F. Cravatt, E.J. Bilsky, D.L. Boger, Reversible competitive alpha-ketoheterocycle inhibitors of fatty acid amide hydrolase containing additional conformational constraints in the acyl side chain: orally active, long-acting analgesics, J. Med. Chem. 54 (2011) 2805–2822.
[20] K. Otrubova, M. Brown, M.S. McCormick, G.W. Han, S.T. O'Neal, B.F. Cravatt, R.C. Stevens, A.H. Lichtman, D.L. Boger, Rational design of fatty acid amide hydrolase inhibitors that act by covalently bonding to two active site residues, J. Am. Chem. Soc. 135 (2013) 6289–6299.
[21] G. Palermo, P. Campomanes, M. Neri, D. Piomelli, A. Cavalli, U. Rothlisberger, M. De Vivo Wagging, The tail: essential role of substrate flexibility in FAAH Catalysis, J. Chem. Theory Comput. 9 (2013) 1202–1213.
[22] R.A. Laskowski, M.B. Swindells, LigPlot+: multiple ligand-protein interaction diagrams for drug discovery, J. Chem. Inf. Model 51 (2011) 2778–2786.
[23] J.L. Knight, C.L. 3rd Brooks, Lambda-dynamics free energy simulation methods, J. Comput. Chem. 30 (11) (2009) 1692–1700.
[24] M. Cipriano, E. Björklund, A.A. Wilson, C. Congiu, V. Onnis, C.J. Fowler, Inhibition of fatty acid amide hydrolase and cyclooxygenase by the N-(3-methylpyridin-2-yl)amide derivatives of flurbiprofen and naproxen, Eur. J. Pharmacol. 720 (1–3) (2013) 383–390.
[25] I.H. Segel, Enzyme Kinetics. Behaviour and Analysis of Rapid Equilibrium and Steady-state Enzyme Systems, John Wiley & Sons, New York, 1975.
[26] K.B.A.S. Bahnck, Y. Tao, S.C. Lilley, M.P. Andrews, G.E. Aspnes, D.J. Bernhardson, D.R. Bill, M.W. Bundesmann, R.L. Dow, K. Karki, T. Le, Q. Li, M.J. Munchhof, A. Nematalla, M. Nihlawi, L. Patel, C. Perreault, M. Waldo, Efficient synthesis of 4-Amino-2-methoxy-7,8-dihydropyrido[4,3-d]pyrimidin-5-ones: practical access to a novel chemotype in the development of DGAT-1 inhibitors, Synthesis 44 (2012) 3152–3157.
[27] M.M. Bradford, A rapid and sensitive method for the quantitation of microgram quantities of protein utilizing the principle of protein-dye binding, Anal. Biochem. 72 (1976) 248–254.
[28] L. Boldrup, S.J. Wilson, A.J. Barbier, C.J. Fowler, A simple stopped assay for fatty acid amide hydrolase avoiding the use of a chloroform extraction phase, J. Biochem. Biophys. Methods 60 (2004) 171–177.
[29] C.J. Fowler, G. Tiger, G.M.L. López-Rodríguez, A. Viso, S. Ortega-Gutiérrez, J.A. Ramos, Inhibition of fatty acid amidohydrolase, the enzyme responsible for the metabolism of the endocannabinoid anandamide, by analogues of arachidonoyl-serotonin, J. Enzyme Inhib. Med. Chem. 18 (2003) 225–231.
[30] B. Paylor, S. Holt, C.J. Fowler, The potency of the fatty acid amide hydrolase inhibitor URB597 is dependent upon the assay pH, Pharmacol. Res. 54 (2006) 481–485. Erratum published in Pharmacol. Res., 55 (2007) 480.
[31] S. Kathuria, S. Gaetani, D. Fegley, F. Valiño, A. Duranti, A. Tontini, M. Mor, G. Tarzia, La G. Rana, A. Calignano, A. Giustino, M. Tattoli, M. Palmery, V. Cuomo, D. Piomelli, Modulation of anxiety through blockade of anandamide hydrolysis, Nat. Med. 9 (2003) 76–81.
[32] A.D. Favia, D. Habrant, R. Scarpelli, M. Migliore, C. Albani, S.M. Bertozzi, M. Dionisi, G. Tarozzo, D. Piomelli, A. Cavalli, M. De Vivo, Identification and characterization of carprofen as a multitarget Fatty Acid amide hydrolase/cyclooxygenase inhibitor, J. Med. Chem. 55 (2012) 8807–8826.
[33] T. Bisogno, D. Melck, L. De Petrocellis, M. Bobrov, N.M. Gretskaya, V.V. Bezuglov, N. Sitachitta, W.H. Gerwick, V. Di Marzo, Arachidonoylserotonin and other novel inhibitors of fatty acid amide hydrolase, Biochem. Biophys. Res. Commun. 248 (1998) 515–522.
[34] E.A. Meade, W.L. Smith, D.L. DeWitt, Differential inhibition of prostaglandin Endoperoxide synthase (cyclooxygenase) isozymes by aspirin and other non-Steroidal anti-inflammatory drugs, J. Biol. Chem. 268 (1993) 6610–6614.
[35] V. Onnis, C. Congiu, E. Björklund, F. Hempel, E. Söderström, C.J. Fowler, Synthesis and evaluation of paracetamol esters as novel fatty acid amide Hydrolase inhibitors, J. Med. Chem. 53 (2010) 2286–2298.
[36] G.M. Morris, R. Huey, W. Lindstrom, M.F. Sanner, R.K. Belew, D.S. Goodsell, A.J. Olson, Autodock4 and AutoDockTools4: automated docking with selective receptor flexiblity, J. Comput. Chem. 16 (2009) 2785–2791.
[37] D.J. Gustin, Z. Ma, X. Min, Y. Li, C. Hedberg, C. Guimaraes, A.C. Porter, M. Lindstrom, D. Lester-Zeiner, G. Xu, T.J. Carlson, S. Xiao, C. Meleza, R. Connors, Z. Wang, F. Kayser, Identification of potent, noncovalent fatty acid amide hydrolase (FAAH) inhibitors, Bioorg. Med. Chem. Lett. 21 (2011) 2492–2496.
[38] M.K. McKinney, B.F. Cravatt, Structure and function of fatty acid amide hydrolase, Annu. Rev. Biochem. 74 (2005) 411–432.
[39] D.A. Case, J.T. Berryman, R.M. Betz, D.S. Cerutti, T.E. Cheatham 3rd, T.A. Darden, R.E. Duke, T.J. Giese, H. Gohlke, A.W. Goetz, N. Homeyer, S. Izadi, P. Janowski, J. Kaus, A. Kovalenko, T.S. Lee, S. LeGrand, P. Li, T. Luchko, R. Luo, B. Madej, K.M. Merz, G. Monard, P. Needham, H. Nguyen, H.T. Nguyen, I. Omelyan, A. Onufriev, D.R. Roe, A. Roitberg, R. Salomon-Ferrer, C.L. Simmerling, W. Smith, J. Swails, R.C. Walker, J. Wang, R.M. Wolf, X. Wu, D.M. York, P.A. Kollman, AMBER 2015, University of California, San Francisco, 2015.
[40] K. Lindorff-Larsen, S. Piana, K. Palmo, P. Maragakis, J.L. Klepeis, R.O. Dror, D.E. Shaw, Improved side-chain torsion potentials for the Amber ff99SB protein force field, Proteins 78 (2010) 1950–1958.
[41] C.I. Bayly, P. Cieplak, W.D. Cornell, P.A. Kollman, A well-behaved electrostatic potential based method using charge restraints for deriving atomic charges, J. Phys. Chem. 97 (1993) 10269–10280.
[42] Gaussian 09, Revision D.01, M.J. Frisch, G.W. Trucks, H.B. Schlegel, G.E. Scuseria, M.A. Robb, J.R. Cheeseman, G. Scalmani, V. Barone, B. Mennucci, G.A. Petersson, H. Nakatsuji, M. Caricato, X. Li, H.P. Hratchian, A.F. Izmaylov, J. Bloino, G. Zheng, J.L. Sonnenberg, M. Hada, M. Ehara, K. Toyota, R. Fukuda, J. Hasegawa, M. Ishida, T. Nakajima, Y. Honda, O. Kitao, H. Nakai, T. Vreven, J.A.Jr. Montgomery, J.E. Peralta, F. Ogliaro, M. Bearpark, J.J. Heyd, E. Brothers, K.N. Kudin, V.N. Staroverov, R. Kobayashi, J. Normand, K. Raghavachari, A. Rendell, J.C. Burant, S.S. Iyengar, J. Tomasi, M. Cossi, N. Rega, J.M. Millam, M. Klene, J.E. Knox, J.B. Cross, V. Bakken, C. Adamo, J. Jaramillo, R. Gomperts, R.E. Stratmann, O. Yazyev, A.J. Austin, R. Cammi, C. Pomelli, J.W. Ochterski, R.L. Martin, K. Morokuma, V.G. Zakrzewski, G.A. Voth, P. Salvador, J.J. Dannenberg, S. Dapprich, A.D. Daniels, Ö. Farkas, J.B. Foresman, J.V. Ortiz, J. Cioslowski, and D.J. Fox, Gaussian, Inc., Wallingford CT, 2009.
[43] B.R. Miller 3rd, T.D. McGee Jr., J.M. Swails, N. Homeyer, H. Gohlke, A.E. Roitberg, MMPBSA.py: an efficient program for end-state free energy calculations, J. Chem. Theory Comput. 8 (2012) 3314–3321.
[44] T. Steinbrecher, I. Joung, D.A. Case, Soft-core potentials in thermodynamic integration: comparing one- and two-step transformations, J. Comput. Chem. 32 (15) (2011) 3253–3263.
[45] Amber 15 Reference Manual, 2015. http://ambermd.org/doc12/Amber15.pdf.
[46] M. Biasini, S. Bienert, A. Waterhouse, K. Arnold, G. Studer, T. Schmidt, F. Kiefer, T. Gallo Cassarino, M. Bertoni, L. Bordoli, T. Schwede, SWISS-MODEL: modelling protein tertiary and quaternary structure using evolutionary information, Nucleic Acids Res. 42 (2014) W252–W258.